

Modeling of the Magnetic Susceptibilities of the Ambient- and High-Pressure Phases of $(\text{VO})_2\text{P}_2\text{O}_7$

D. C. Johnston

Ames Laboratory and Department of Physics and Astronomy, Iowa State University, Ames, Iowa 50011

T. Saito, M. Azuma, and M. Takano

Institute for Chemical Research, Kyoto University, Uji, Kyoto-fu 611-0011, Japan

T. Yamauchi and Y. Ueda

Institute for Solid State Physics, University of Tokyo, 7-22-1 Roppongi, Minato-ku, Tokyo 106-8666, Japan
(November 1, 2018)

The magnetic susceptibilities χ versus temperature T of powders and single crystals of the ambient-pressure (AP) and high-pressure (HP) phases of $(\text{VO})_2\text{P}_2\text{O}_7$ are analyzed using an accurate theoretical prediction of $\chi(T, J_1, J_2)$ for the spin-1/2 antiferromagnetic alternating-exchange (J_1, J_2) Heisenberg chain. The results are consistent with recent models with two distinct types of alternating-exchange chains in the AP phase and a single type in the HP phase. The spin gap for each type of chain is derived from the respective set of two fitted alternating exchange constants and the one-magnon dispersion relation for each of the two types of chains in the AP phase is predicted. The influences of interchain coupling on the derived intrachain exchange constants, spin gaps, and dispersion relations are estimated using a mean-field approximation for the interchain coupling. The accuracies of the spin gaps obtained using fits to the low- T $\chi(T)$ data by theoretical low- T approximations are determined. The results of these studies are compared with previously reported estimates of the exchange couplings and spin gaps in the AP and HP phases and with the magnon dispersion relations in the AP phase measured previously using inelastic neutron scattering.

PACS numbers: 75.50.Ee, 75.40.Cx, 75.30.Et, 75.10.Jm

I. INTRODUCTION

A resurgence of research on the magnetic properties of low-dimensional quantum spin systems has occurred over the last decade. This work was mainly initially undertaken to understand the relationships between the magnetic properties of layered cuprates containing Cu^{+2} spin-1/2 square lattice layers and the high superconducting transition temperatures of the doped materials.¹ This goal has also spawned much research on related one- and two-dimensional (1D and 2D) spin systems. Indeed, the new subfield of spin ladder physics was created as a result of these efforts.^{2,3} The basic n -leg spin ladder consists of a planar arrangement of n parallel vertical spin chains (the ladder “legs”) with (nonfrustrating) horizontal nearest neighbor couplings between adjacent chains, i.e., across the ladder “rungs”.

Self-doped two-leg spin ladders are realized in the compound NaV_2O_5 , in which the V atoms are crystallographically equivalent and the oxidation state of the V atoms is +4.5, resulting formally in a mixed-valent $d^{0.5}$ system.⁴ However, the material is a semiconductor rather than a metal. Theoretical studies have indicated that the reason for this is that the one d electron per two V atoms is localized on the respective V-O-V rung of the ladder due to the on-site Coulomb repulsion on each rung. This in turn led to the hypothesis that each rung acts as a spin-1/2 site, in which case the compound is expected to

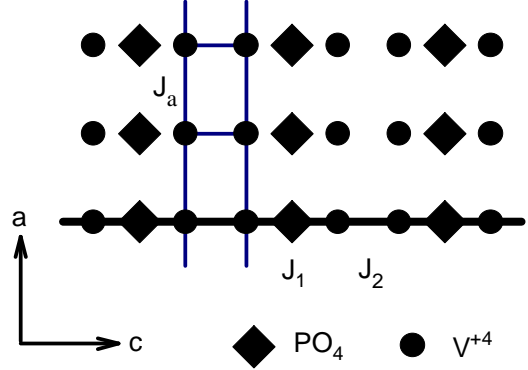


FIG. 1. Sketch of the basic structures of AP- $(\text{VO})_2\text{P}_2\text{O}_7$ and HP- $(\text{VO})_2\text{P}_2\text{O}_7$ in the a - c plane, showing the exchange constants J_1 and J_2 along the spin-1/2 V^{+4} alternating-exchange chains and J_a in a perpendicular direction along the legs of the structural two-leg ladders (adapted from Ref. 11). The lattice parameters of AP- $(\text{VO})_2\text{P}_2\text{O}_7$ are $a \approx 7.74$, $b \approx 9.59$, and $c \approx 16.59$ Å, and of HP- $(\text{VO})_2\text{P}_2\text{O}_7$ are $a \approx 7.58$, $b \approx 9.55$, and $c \approx 8.36$ Å.

behave magnetically like a spin $S = 1/2$ antiferromagnetic (AF) Heisenberg chain. Additionally, the observation of a spin dimerization transition below 34 K, accompanied by a lattice distortion, is consistent with this scenario. These and other aspects of the thermal and magnetic behaviors of NaV_2O_5 were recently examined in

detail in a combined theoretical and experimental study.⁵ As part of this study, an accurate function was generated for the theoretical magnetic susceptibility χ versus temperature T of the spin $S = 1/2$ AF alternating-exchange (J_1 and J_2 with $J_2 \leq J_1$) Heisenberg chain over the entire range $0 \leq \alpha \leq 1$ of the alternation parameter $\alpha \equiv J_2/J_1$.

The availability of this high-accuracy theoretical $\chi(k_B T/J_1, \alpha)$ function now allows one to accurately and precisely test the consistency of proposals for the occurrence of alternating-exchange chains in specific compounds by comparing the observed $\chi(T)$ with that expected theoretically. In particular, in the present work we use this method to test the consistency of recently

proposed alternating-exchange chain models for the ambient- and high-pressure phases of vanadyl pyrophosphate, $(VO)_2P_2O_7$, and we obtain the exchange constants and spin gaps in the respective chains. The influence of interchain coupling on the derived intrachain exchange constants and spin gaps is investigated using a mean-field approximation for the interchain coupling. The accuracies of the spin gaps obtained using fits to the low- T $\chi(T)$ data by theoretical low- T approximations are determined. The results of these studies are compared with previously reported estimates of the exchange couplings and spin gaps in the two phases and with the dispersion relations measured for the ambient-pressure

TABLE I. Spectroscopic splitting factor (g -factor) g , exchange constants J_1 and J_2 and spin gap Δ determined by the method listed for the ambient-pressure form of $(VO)_2P_2O_7$ [AP- $(VO)_2P_2O_7$], for the high pressure form HP- $(VO)_2P_2O_7$ and for the V dimer compound $(VO)HPO_4 \cdot \frac{1}{2}H_2O$. Quantities marked with a dagger (\dagger) are derived using the $S = 1/2$ alternating-exchange chain model whereas those marked by an asterisk (*) are derived using the $S = 1/2$ two-leg ladder model. Quantities with no mark make no assumption about the specific model and/or are determined or assumed independently of the fits used to obtain the other listed quantities. All measurements were carried out on polycrystalline samples except as otherwise noted. The listed alternating exchange constants from Ref. 24 were obtained within a 2D coupled alternating-exchange chain model with interchain couplings given in the text and were determined from a fit to one-magnon inelastic neutron scattering data (Ref. 11) with the spin gap listed and from high- T $\chi(T)$ data (Ref. 10). The error bars on the parameters listed from the present work include the estimated influences of interchain interactions.

Compound	g	α	J_1/k_B (K)	J_2/k_B (K)	Δ/k_B (K)	Method	Ref.	
AP- $(VO)_2P_2O_7$	2.00 \dagger	0.7 \dagger	131 \dagger	92 \dagger		$\chi(T)$	10	
	1.99 \dagger	0.722 \dagger	128.9 \dagger	93.0 \dagger	57 \dagger	$\chi(T)$	14	
	2.03*	1.007*	90.6*	90.0*	45.7*	$\chi(T)$	14	
					30	$^{31}K(T)$	15	
					60	$^{31}(1/T_1)(T)$	15	
					34(3)	$^{31}K(T)$	16	
					100	$^{31}(1/T_1)(T)$	16	
					52	$\chi(T)$	17	
					43(2)	0_n scatt.	18	
	crystal	1.937			35	$c_{11}(H, 1.6 K)$	19	
	crystal				36	Raman (low T)	20	
	crystals					40.4(4), 70	0_n scatt.	21
						36.2(3), 66.7(2)	0_n scatt.	11
			1.97			33(1), 62(3)	$M(H, 1.3 K)$	26
					35(2), 52(3)	$^{31}K(T)$	26	
					53, 71	$^{31}(1/T_1)(T)$	27	
					68(2)	$^{51}K(T)$	27	
crystal crystal		0.83 \dagger , 0.67 \dagger	124 \dagger , 136 \dagger	103 \dagger , 92 \dagger	35, 68	$^{51}(1/T_1)(T)$ Inferred	27 27	
		0.793 \dagger	124 \dagger	99 \dagger	36.2(3)	Theory	24	
		0.67 \dagger	122 \dagger	82 \dagger	58 \dagger	$\chi(T \approx 70 K)$	22	
					67	ESR $I(T)$	22	
		2.021(2) \dagger	0.782(2) \dagger	130.9(5) \dagger	102.4(6) \dagger		$\chi(T)$	13
			0.85(1) \dagger , 0.638(7) \dagger	135(5) \dagger , 127(3) \dagger	115(6) \dagger , 81(3) \dagger	38.4(9) \dagger , 67(1) \dagger	$\chi(T)$	This work
	HP- $(VO)_2P_2O_7$	2				23	$M(H, 1.3 K)$	30
						27	$\chi(T < 30 K)$	30
		2.01 \dagger	0.9 \dagger	137 \dagger	123 \dagger	27 \dagger	$\chi(T > 30 K)$	30
	crushed crystals		0.8737(13) \dagger	135.6(7) \dagger	118.5(8) \dagger	33.9(2) \dagger	$\chi(T)$	This work
$(VO)HPO_4 \cdot \frac{1}{2}H_2O$	1.99	0	88.0	0	88.0	$\chi(T)$	9	
					74	$^{31}K(T)$	15	
		0	90.6(5)	0	90.6(5)	0_n scatt.	23	

phase by inelastic neutron scattering.

The history of the study of the magnetic properties of $(\text{VO})_2\text{P}_2\text{O}_7$ is interesting and extensive. In the following two sections we give brief overviews of the previous work on the ambient-pressure (AP) and high-pressure (HP) phases of this compound, respectively, and then present the plan for the remainder of the paper.

A. AP- $(\text{VO})_2\text{P}_2\text{O}_7$

The V^{+4} d^1 ambient-pressure phase AP- $(\text{VO})_2\text{P}_2\text{O}_7$, sometimes abbreviated in the recent literature as “VOPO”, is an industrial catalyst for the selective oxidation of n -butane to maleic anhydride.^{6,7} This compound was found to have an orthorhombic crystal structure^{8,9} (containing four inequivalent types of V atoms) which can be viewed crystallographically as containing $S = 1/2$ two-leg ladders,¹⁰ where the rungs of the ladder lie along the c -axis and the legs are oriented along the a -axis, as sketched in Fig. 1.¹¹ A single crystal x-ray diffraction structural study claimed that the previous structural studies were incorrect and that the structure is monoclinic with eight inequivalent V atoms in the unit cell, although the overall structural features and the unit cell dimensions were found to be very similar to those of the previously proposed orthorhombic structure.¹² However, a recent study of a polycrystalline sample using both x-ray and neutron diffraction Rietveld refinements and transmission electron microscopy confirmed the orthorhombic structure and ruled out the monoclinic structure;¹³ it was suggested that whether the orthorhombic or monoclinic structure occurs in a particular sample may depend on the exact composition and the details of sample synthesis.¹³ There have been two conventions used in the literature for designating the b and c axes in which these two axes are mutually interchanged; we will adhere to the convention in Fig. 1, as in Ref. 13, for which the approximate lattice parameters are listed in the figure caption.

The magnetic susceptibility versus temperature $\chi(T)$ of AP- $(\text{VO})_2\text{P}_2\text{O}_7$ was found to exhibit an energy gap (“spin gap”) for magnetic excitations.¹⁰ The $\chi(T)$ was initially fitted to high precision by the prediction for the $S = 1/2$ AF alternating-exchange Heisenberg chain, with the exchange constants J_1 and J_2 and alternation parameter $\alpha \equiv J_2/J_1$ given in Table I.¹⁰ A fit by the spin ladder model as suggested¹⁰ from the crystal structure (see Figs. 1 and 2) was not possible at that time (1987) due to lack of theoretical predictions for $\chi(T)$ of this model. It was also speculated that even though the crystallographic features suggest a spin ladder model, the actual magnetic interactions might turn out to correspond to those of alternating-exchange spin chains.¹⁰ When $\chi(T)$ calculations for the spin ladder model were eventually done,¹⁴ it was found that the same experimental $\chi(T)$ data set¹⁰ could be fitted by the spin lad-

der model to the same high precision as for the very different alternating-exchange chain model.¹⁴ The existence of a spin gap was subsequently confirmed and its value estimated from NMR measurements of the ^{31}P Knight shift $^{31}K(T)$ and nuclear spin-lattice relaxation rate $^{31}(1/T_1)(T)$,^{15,16} from $\chi(T)$ (Ref. 17) and inelastic neutron scattering¹⁸ measurements on polycrystalline samples at low temperatures, and most recently from elastic constant measurements¹⁹ on a single crystal in pulsed magnetic fields up to 50 T at $T = 1.6$ K and from Raman scattering intensity measurements on single crystals at low temperatures,²⁰ as listed in Table I.

The above inelastic neutron scattering measurements on polycrystalline AP- $(\text{VO})_2\text{P}_2\text{O}_7$ reportedly confirmed the spin ladder model and rejected the alternating-exchange chain model by a comparison of the observed spin gap [43(2) K] with the values 45.7 K and 57 K predicted for the two respective models from the sets of exchange constants determined from respective fits to the $\chi(T)$ data.¹⁸ However, subsequent inelastic neutron scattering results on polycrystalline samples²¹ and especially on a collection of about 200 oriented small single crystals¹¹ proved that AP- $(\text{VO})_2\text{P}_2\text{O}_7$ is not a spin-ladder compound. The strongest dispersion of the one-magnon spectra of the single crystals was found to be along the c axis, i.e., in the direction of the structural ladder rungs, and the coupling in the direction of the ladder legs was found to be weakly ferromagnetic.¹¹ Thus, perhaps surprisingly, the superexchange coupling path V-O-P-O-V along the c axis, coupling the structural two-leg ladders as shown in Fig. 2, is much stronger than the shorter V-O-V coupling along the ladder legs parallel to the a -axis. These results were interpreted in terms of an alternating-exchange chain model with the chains running along the c axis, with weak coupling between the chains, thus confirming the above speculation in Ref. 10. Subsequent $\chi(T)$ data for powder¹³ and single crystal²² samples have been interpreted in terms of the alternating-exchange chain model, with exchange parameters listed in Table I.

The spin gaps of 43(2) K (Ref. 18) and 40.4(4) K (Ref. 21) found from inelastic neutron scattering measurements on powder samples are both significantly larger than the one-magnon spin gap of 36.2(3) K determined from the neutron scattering measurements on single crystals.¹¹ Since powder samples have usually been found to show relatively high levels of paramagnetic impurities and/or defects, this comparison suggests that the larger spin gaps in the powder samples may be a real effect arising from termination of the spin chains by defects. One would indeed expect finite segments of alternating-exchange chains to exhibit larger spin gaps than for the infinite chain.

We have also listed in Table I the intradimer exchange constant determined from $\chi(T)$ (Ref. 9), ^{31}P NMR Knight shift $^{31}K(T)$ (Ref. 15), and inelastic neutron scattering²³ measurements of polycrystalline samples of the d^1 $S = 1/2$ vanadium dimer compound

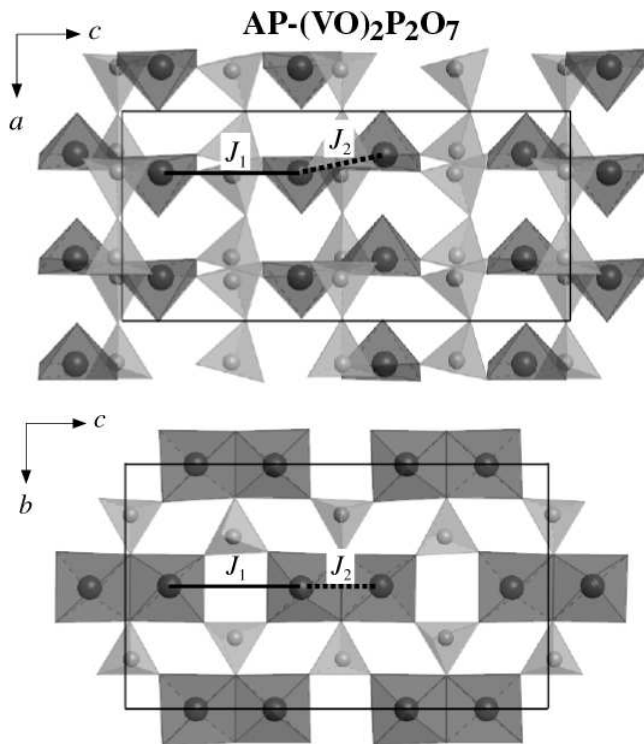


FIG. 2. Detailed crystal structure of AP-(VO)₂P₂O₇ as viewed along the *b*-axis (top panel) and along the *a* axis (bottom panel). The rectangular boxes are outlines of the unit cell in the respective planes. The large spheres are V atoms and the small spheres are P atoms. Oxygen atoms (not shown) are at the vertices of the VO₅ square pyramids and the PO₄ tetrahedra. The pairs of V atoms coupled by exchange constants J_1 and J_2 along the $S = 1/2$ AF alternating-exchange Heisenberg chains are shown.

(VO)HPO₄ · $\frac{1}{2}$ H₂O (vanadyl hydrogen phosphate hemihydrate), which is a precursor for the synthesis of, and has structural similarities to, AP-(VO)₂P₂O₇.^{6,9} In particular, the neutron scattering study of this compound confirmed the importance and strength of the V-O-P-O-V superexchange pathway.²³

From the above neutron scattering measurements on single crystals of AP-(VO)₂P₂O₇, a second spin gap at a larger energy of 67 K was found in addition to the gap of 36 K for coherent one-magnon propagation along the *c* axis.¹¹ The two spin gaps cannot both arise from one-magnon excitations in an isolated alternating-exchange chain and the larger one was suggested to arise from neutron scattering from two-magnon triplet bound states of such chains, although the scattered neutron intensity was larger than expected from scattering from such states.¹¹ A 2D model incorporating both nonfrustrating (J_a , see Fig. 1) and diagonal frustrating (J_\times) AF interactions between alternating-exchange chains was subsequently proposed.²⁴ The intrachain and interchain ex-

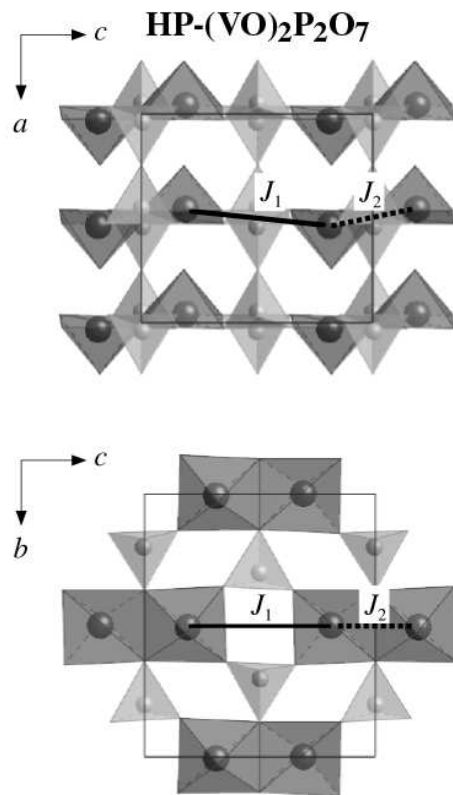


FIG. 3. Detailed crystal structure of HP-(VO)₂P₂O₇. The designations are the same as in Fig. 2.

change constants were determined by a (very good) fit to the one-magnon dispersion relation (including the one-magnon spin gap of 36 K) measured in the inelastic neutron scattering measurements and by using the results¹⁰ of high- T $\chi(T)$ measurements. The two alternating AF intrachain exchange constants so determined²⁴ are listed in Table I. The two AF interchain interactions were predicted to be rather large: $J_a/J_1 = 0.203$ and $J_\times/J_1 = 0.255$.²⁴ However, the $\chi(T)$ calculated using this model in Ref. 24 was found to be in poor agreement with experimental single-crystal $\chi(T)$ data²² even at the highest measured temperature $T \sim 200$ K, which is significantly above the temperature (~ 70 K) at which $\chi(T)$ shows a broad maximum and where the prediction would be expected to be quite accurate. On the other hand, we find in Sec. III B 2 below that their $\chi(T)$ prediction is in quite good agreement with experimental data if the comparison is done in a somewhat different way. Additional calculations indicated that the frustrating AF interchain interaction stabilizes two-magnon bound states and thus supported the conjecture¹¹ that the higher energy mode at 67 K is a triplet two-magnon bound state.²⁴ The same 2D model containing alternating-exchange chains and frustrating AF interchain couplings and also a model con-

taining ferromagnetic interchain couplings were studied in Ref. 25 where the former model was found to agree better with the experimental neutron scattering data. From a Raman scattering study of single crystals, the spin-phonon interaction was suggested to be responsible for the formation of the two-magnon triplet bound states identified in the neutron scattering experiments, rather than arising from frustrating interchain interactions.²⁰

Electron spin resonance (ESR) intensity versus temperature $I(T)$ data obtained for a single crystal were interpreted in terms of an isolated AF spin dimer model, yielding a spin gap of 67 K,²² corresponding to the higher-energy gap seen in the inelastic neutron scattering data. In this ESR study, transitions between the Zeeman levels within the one-magnon triplet band were reportedly not observed. These $I(T)$ data were subsequently reinterpreted within the above 2D coupled alternating-exchange chain model as arising from transitions between the Zeeman levels within the one-magnon band and good agreement between the theoretical prediction for $I(T)$ and the experimental $I(T)$ data was found.²⁴

On the other hand, recent ³¹P and ⁵¹V NMR and magnetization versus applied magnetic field $M(H)$ measurements at high fields and low temperatures have indicated that there are two magnetically distinct types of alternating-exchange V chains in AP-(VO)₂P₂O₇, interpenetrating with each other, each with its own spin gap.^{26,27} The two spin gaps inferred for the two types of chains, 35(2) K from ³¹P $K(T)$ measurements²⁶ and 68(2) K from ⁵¹V $K(T)$ measurements,²⁷ and 33(1) K and 62(3) K from $M(H)$ measurements at 1.3 K,²⁶ agree well with the above two spin gaps found from the neutron scattering measurements, respectively, thus providing an alternate explanation for the larger of the two spin gaps. Using additional information from the neutron scattering one-magnon dispersion relation measurements,¹¹ the two alternating exchange constants in each chain have been estimated²⁷ and are listed in Table I. This model is not supported by the Raman scattering results.²⁰ However, recent unpublished inelastic neutron scattering measurements on a large single crystal at $T = 2$ K in zero and high magnetic fields show that the two types of magnetic excitations found earlier¹¹ split in a magnetic field according to expectation for two triplet bands, results which constitute independent evidence for the validity of the two-chain model for AP-(VO)₂P₂O₇.²⁸ In addition, two previously undetected magnetic excitations termed “shadow bands” were found which are thought to arise from the staggered alignment of successive V dimers along the V alternating-exchange chains within the structure (see the top panel of Fig. 2).^{28,29}

At present there is thus no universal agreement about a Hamiltonian which can self-consistently explain the various experimental measurements probing the magnetism in AP-(VO)₂P₂O₇, although all of the models considered recently contain $S = 1/2$ AF alternating-exchange Heisenberg chains as an essential element and a consen-

sus is emerging that the two-chain model can explain many of the observed properties.

B. HP-(VO)₂P₂O₇

The high-pressure phase HP-(VO)₂P₂O₇ was recently synthesized by heating polycrystalline AP-(VO)₂P₂O₇ for 1/2 h at 700 °C under a pressure of 2 GPa.³⁰ As shown in Fig. 3 and by comparison with Fig. 2, HP-(VO)₂P₂O₇ has a simpler structure than AP-(VO)₂P₂O₇. In HP-(VO)₂P₂O₇, all V atoms are crystallographically equivalent but the same basic structure as in the ambient-pressure phase was found.^{13,30} The similarities between the two structures suggest that HP-(VO)₂P₂O₇ also contains $S = 1/2$ AF alternating-exchange chains, but of a single type.³⁰ Indeed, high-field $M(H)$ measurements at 1.3 K revealed a single spin gap of ~ 23 K, consistent with this hypothesis.³⁰ Modeling of $\chi(T)$ data below 30 K was carried out using the low- T approximation in Eq. (7a) below for the spin susceptibility of a 1D spin system with a spin gap, yielding a similar spin gap of 27 K.³⁰ The $\chi(T)$ data above 30 K were analyzed using the spin susceptibility of the $S = 1/2$ alternating-exchange Heisenberg chain model, yielding the exchange constants listed in Table I and the same spin gap $\Delta/k_B = 27$ K.³⁰ These estimates of the gap value are similar to the one-magnon gap of ≈ 36 K in AP-(VO)₂P₂O₇ found from the inelastic neutron scattering and other measurements discussed above.

Equation (7a) has also been previously used to fit $\chi(T)$ data for other $S = 1/2$ 1D compounds, but to our knowledge all such studies, with the exception of a study of the Cu⁺² $S = 1/2$ two-leg Heisenberg spin ladders in SrCu₂O₃,³¹ have assumed that A and the spin gap Δ are independently adjustable parameters when fitting experimental $\chi(T)$ data. We discuss in Sec. II below that A is uniquely related to Δ and is not an independently adjustable parameter for a given type of 1D spin lattice.⁵ On the other hand, if one assumes that the spin lattice in a material has a spin gap but the type of 1D spin lattice is unknown, or if the fit is not carried out in the low-temperature limit, then A and Δ would have to be treated as independently adjustable parameters. In the present work we evaluate the accuracy of using Eq. (7a) to determine the spin gap of the 1D $S = 1/2$ alternating-exchange Heisenberg chain from $\chi(T)$ data for HP-(VO)₂P₂O₇ by comparing the spin gap obtained using this approximation with the spin gap obtained by modeling the same data set using the accurate theoretical prediction⁵ for the spin susceptibility of the $S = 1/2$ AF alternating-exchange Heisenberg chain model.

Most recently, single crystals of HP-(VO)₂P₂O₇ have been grown.³² The anisotropic spectroscopic splitting factors (g factors) of the $S = 1/2$ V⁺⁴ ions in a single crystal were determined from ESR measurements and the anisotropic magnetic susceptibilities of a single crystal were measured.³² Here we perform detailed modeling of

these $\chi(T)$ data using the g factors determined from ESR and using the $S = 1/2$ AF alternating-exchange Heisenberg chain model for the spin susceptibility. We determine the exchange constants within the chains and from these we obtain an estimate of the spin gap. An independent estimate of the spin gap is obtained by modeling only the low-temperature data.

C. Plan of the Paper

The plan for the remainder of this paper is as follows. In Sec. II a summary is given of the theory that we will need to carry out and discuss the modeling described above. General considerations for fitting experimental data by theoretical predictions for the spin susceptibility are discussed in Sec. III A. New and literature $\chi(T)$ data for AP-(VO)₂P₂O₇ are presented and fitted in Sec. III B. High-precision fits to the $\chi(T)$ of a high-purity powder sample are presented in Sec. III B 1. In this section, we show how the fitted exchange constants and spin gap(s) of the model of alternating-exchange chain(s) vary depending on whether a single-chain or two-chain model is used to fit the data, and on whether the g value is fixed or allowed to vary during the fits. The influences of interchain couplings on the exchange constants and spin gaps inferred from modeling $\chi(T)$ for the powder sample are quantitatively determined in Sec. III B 2 using a molecular field theory for the interchain couplings, where we also compare our derived interchain couplings with the corresponding theoretical predictions of Uhrig and Normand²⁴ which were obtained using a one-chain model. The $\chi(T)$ data for two single crystals of AP-(VO)₂P₂O₇ are analyzed using the two-chain model in Sec. III B 3. In Sec. III C we test our predicted dispersion relations for the two proposed chains by comparison with the results of inelastic neutron scattering measurements. The $\chi(T)$ data for HP-(VO)₂P₂O₇ are presented and modeled in Sec. III D. The most accurate and precise $\chi(T)$ data for this phase were obtained for a sample of crushed crystals. These data are analyzed using the one-chain model in Sec. III D 1. The influences of interchain couplings on the derived exchange constants and spin gap of this sample are considered in Sec. III D 2. Our evaluation of the accuracy of the spin gap obtained using a theoretical low- T approximation to the spin susceptibility of a 1D $S = 1/2$ spin system with a spin gap, as previously used to analyze powder $\chi(T)$ data for HP-(VO)₂P₂O₇,³⁰ is given in Sec. III D 3. The anisotropic $\chi(T)$ data³² for a single crystal of HP-(VO)₂P₂O₇ are modeled in Sec. III D 4. The powder average of these single crystal $\chi(T)$ data are modeled in Sec. III D 5 by two low- T approximations for the spin susceptibility to obtain an independent estimate of the spin gap. A summary of our modeling results and our conclusions are given in Sec. IV.

II. THEORY

The Hamiltonian for the $S = 1/2$ alternating-exchange Heisenberg chain is written in three equivalent ways as

$$\mathcal{H} = \sum_i J_1 \mathbf{S}_{2i-1} \cdot \mathbf{S}_{2i} + J_2 \mathbf{S}_{2i} \cdot \mathbf{S}_{2i+1} \quad (1a)$$

$$= \sum_i J_1 \mathbf{S}_{2i-1} \cdot \mathbf{S}_{2i} + \alpha J_1 \mathbf{S}_{2i} \cdot \mathbf{S}_{2i+1} \quad (1b)$$

$$= \sum_i J(1 + \delta) \mathbf{S}_{2i-1} \cdot \mathbf{S}_{2i} + J(1 - \delta) \mathbf{S}_{2i} \cdot \mathbf{S}_{2i+1}, \quad (1c)$$

where

$$J_1 = J(1 + \delta) = \frac{2J}{1 + \alpha}, \quad (2a)$$

$$\alpha = \frac{J_2}{J_1} = \frac{1 - \delta}{1 + \delta}, \quad (2b)$$

$$\delta = \frac{J_1}{J} - 1 = \frac{J_1 - J_2}{2J} = \frac{1 - \alpha}{1 + \alpha}, \quad (2c)$$

$$J = \frac{J_1 + J_2}{2} = J_1 \frac{1 + \alpha}{2}, \quad (2d)$$

with AF couplings $J_1 \geq J_2 \geq 0$, $0 \leq (\alpha, \delta) \leq 1$. The uniform undimerized chain corresponds to $\alpha = 1$, $\delta = 0$ and $J_1 = J_2 = J$, whereas the isolated dimer has $\alpha = 0$, $\delta = 1$, $J_2 = 0$ and intradimer exchange interaction J_1 . The form of the Hamiltonian in Eq. (1c), in which the appropriate variables are δ and the average exchange constant along the chain J instead of α and the maximum exchange constant J_1 as in Eq. (1b), is often used for compounds in which the spin dimerization is weak and/or for systems showing a second-order spin dimerization transition with decreasing temperature such as occurs in spin-Peierls systems.

The spin gap Δ for magnetic spin excitations from the $S = 0$ ground state to the lowest-lying $S = 1$ triplet excited states for the alternating-exchange chain is uniquely related to the alternation parameter α and the larger exchange constant J_1 (or equivalently to δ and J). The ratio $\Delta(\alpha)/J_1$ for the $S = 1/2$ AF alternating-exchange Heisenberg chain was computed to high ($\leq 1\%$) accuracy for $0 \leq \alpha \leq 0.9$, in α increments of 0.1, using multi-precision methods by Barnes, Riera and Tennant.³³ They found that their calculations could be parametrized very well by the simple expression

$$\frac{\Delta(\alpha)}{J_1} \approx (1 - \alpha)^{3/4} (1 + \alpha)^{1/4}, \quad (3a)$$

or equivalently

$$\frac{\Delta(\delta)}{J} \approx 2 \delta^{3/4}. \quad (3b)$$

An expression for $\Delta(\delta)/J$ which is thought to be more accurate (± 0.0002) over the entire range $0 \leq \delta \leq 1$, obtained by fitting numerical $\Delta(\delta)/J$ data by a generalized form of Eq. (3b), is⁵

$$\frac{\Delta(\delta)}{J} = 2\delta^{y(\delta)}, \quad (4a)$$

where the exponent $y(\delta)$ is given by

$$y(\delta) = y(1) + n_1 \tanh \left[\frac{\ln \delta}{m_1} \ln \left(\frac{\ln \delta}{m_2} \right) \right] + n_2 \tanh^2 \left[\frac{\ln \delta}{m_1} \ln \left(\frac{\ln \delta}{m_2} \right) \right] \quad (4b)$$

with parameters

$$y(1) = 0.74922, \quad n_1 = 0.00776, \quad n_2 = -0.00685, \\ m_1 = 3.3297, \quad m_2 = -2.2114. \quad (4c)$$

The expression for $\Delta(\delta)/J$ in Eqs. (4) can be transformed into an expression for $\Delta(\alpha)/J_1$ using the conversion expressions (2).

For notational convenience, we define the reduced spin susceptibility χ^* , reduced temperature t and reduced spin gap Δ^* as

$$\chi^* \equiv \frac{\chi^{\text{spin}} J_1}{N g^2 \mu_B^2}, \quad t \equiv \frac{k_B T}{J_1}, \quad \Delta^* = \frac{\Delta}{J_1}, \quad (5)$$

where χ^{spin} is the spin susceptibility, N is the number of spins, k_B is Boltzmann's constant and χ^* depends on both t and the alternating exchange parameter $\alpha \equiv J_2/J_1$.

An accurate but unwieldy two-dimensional function $\chi^*(t, \alpha)$ for the $S = 1/2$ AF alternating-exchange Heisenberg chain has been derived for the entire range $0 \leq \alpha \leq 1$ of the alternation parameter by a global fit to numerical quantum Monte Carlo (QMC) simulations and transfer-matrix density-matrix renormalization group (TMRG) and Bethe ansatz $\chi^*(t, \alpha)$ calculations,⁵ which we will not reproduce here but will explicitly use to model $\chi(T)$ data for both AP- and HP-(VO)₂P₂O₇. The absolute accuracy of this function for $0 \leq \alpha \leq 1$ and $0.01 \lesssim t$ is estimated to be $\lesssim 2 \times 10^{-4}$, which corresponds to $\lesssim 0.1\%$ of the susceptibility at the broad maximum. For practical purposes of fitting experimental $\chi(T)$ data, this function can be considered to be exact for $t \gtrsim 0.01$.

Troyer, Tsunetsugu, and Würtz³⁴ have derived a general expression for the low- T limit of $\chi^*(t)$ for a one-dimensional spin system with a spin gap, assuming that (i) the one-magnon dispersion relation is nondegenerate (apart from the Zeeman degeneracy), (ii) the lowest magnetic excited states are one-magnon $S = 1$ triplet excitations, (iii) $k_B T \ll \Delta$ and $k_B T \ll$ one-magnon bandwidth, and (iv) the one-magnon dispersion relation $E(k)$ is parabolic near the minimum according to (in the present notation)

$$\varepsilon_k \equiv \frac{E(k)}{J_1} = \Delta^* + c^*(ka)^2, \quad (6)$$

where k is the wavevector in the direction of the 1D system and a is the (average) nearest-neighbor spin-spin distance. These assumptions hold for the present case of the $S = 1/2$ AF alternating-exchange Heisenberg chain except for the limit $\alpha = 0$ as discussed below and for $\alpha = 1$ for which $\Delta = 0$.⁵ With these four assumptions, $\chi^*(t)$ is given by³⁴

$$\chi^*(t) = \frac{A}{\sqrt{t}} e^{-\Delta^*/t}, \quad (t \ll \Delta^*, \text{ bandwidth}/J_1) \quad (7a)$$

with

$$A = \frac{1}{2\sqrt{\pi c^*}}. \quad (7b)$$

The dimensionless dispersion parameter c^* in Eq. (6) has a unique relationship to the reduced spin gap Δ^* for any given 1D spin system. For example, according to the model of Ref. 5, this relationship for the $S = 1/2$ AF alternating-exchange Heisenberg chain gives the value of the parameter A in Eq. (7a) as

$$A = \frac{\sqrt{\Delta^*}}{\sqrt{2\pi} f(\Delta^*)}, \quad (8)$$

which in turn yields the low- T limit of $\chi^*(t)$ in Eq. (7a) as

$$\chi^*(t) = \frac{1}{\sqrt{2\pi} f(\Delta^*)} \left(\frac{\Delta^*}{t} \right)^{1/2} e^{-\Delta^*/t}, \quad (t \ll \Delta^*) \quad (9a)$$

where the dimensionless function $f(\Delta^*)$ is the solution of

$$\text{E} \left[- \frac{f^2(\Delta^*)}{\Delta^{*2}} \right] = \frac{\pi}{2\Delta^*} \quad (9b)$$

and $\text{E}(x)$ is the complete elliptic integral of the second kind.

From Eq. (8), the parameter A in Eq. (7a) is not an independently adjustable parameter but instead is a unique function of the reduced spin gap Δ^* ,⁵ as was also previously inferred for two-leg spin ladders.³¹ In addition, we see from Eq. (9a) that the two independent parameters of $\chi^*(t, \alpha) \equiv \chi^*(k_B T/\Delta, \Delta/J_1)$. Finally, and perhaps most importantly, the high-temperature limit of the low-temperature regime in which $\chi^*(t)$ is closely approximated by Eqs. (9) is of order $\Delta^*/10$.⁵ At such low temperatures $\chi(T)$ is immeasurably small, and hence the spin gap obtained by analyzing experimental $\chi(T)$ data for various compounds up to temperatures corresponding to a sizable fraction of Δ^* using Eq. (7a) leads to fitted spin gap values which may be significantly different from the actual spin gaps.

The result for the low- t limit of $\chi^*(t)$ in Eq. (7a) is not valid for the isolated dimer, which is one limit of the alternating-exchange chain with $\alpha = J_2 = 0$, because the assumption (iii) that $k_B T \ll$ one-magnon bandwidth

required for that equation to hold is violated at all finite temperatures. For the isolated dimer, the one-magnon bandwidth is identically zero and the reduced spin gap is $\Delta^* = 1$. The reduced spin susceptibility is given exactly by

$$\chi^{*,\text{dimer}}(t) = \frac{1}{t(3 + e^{1/t})} \quad (10a)$$

with the low-temperature limit

$$\chi^{*,\text{dimer}}(t) = \frac{1}{t} e^{-1/t} \quad (t \ll 1). \quad (10b)$$

The temperature dependence of the prefactor to the exponential term in Eq. (10b) is different from that in Eq. (7a). As discussed in Ref. 5, a crossover occurs with decreasing temperature at low temperatures in the effective prefactor from a $1/t$ dependence to a $1/\sqrt{t}$ dependence if $0 < \alpha \ll 1$.

As noted above, the form for the low- T behavior of the spin susceptibility in Eq. (7a) is valid only at very low temperatures. Many years ago, Bulaevskii found that his numerical values of $\chi^*(t, \alpha)$ for the $S = 1/2$ AF alternating-exchange Heisenberg chain, computed from an analytic theory based on the Hartree-Fock approximation, could be fitted over a relatively large temperature interval $0.033 \leq t \leq 1/4$ by³⁵

$$\chi^*(t) = \frac{A}{t} e^{-\Delta^*/t}, \quad (11)$$

and he tabulated A and Δ^* versus the alternation parameter α . A recent extensive numerical study⁵ of his theory confirmed that the numerical predictions of his theory in the above-cited low-temperature range are fitted better by the form (11) than by (7a). In addition, this study showed that although the fitting parameter $\Delta^*(\alpha)$ approximately follows the actual spin gap of Bulaevskii's theory, significant discrepancies occur.⁵ Finally, a detailed numerical comparison of the prediction of Bulaevskii's theory for $\chi^*(t, \alpha)$ with QMC simulations and TMRG calculations of this quantity showed that Bulaevskii's theory is unsuitable for accurately extracting α values from experimental $\chi(T)$ data when $\alpha \lesssim 1$.⁵

For Heisenberg spin lattices consisting of identical spin subsystems with susceptibility $\chi_0^*(t)$ which are weakly coupled to each other, the molecular field theory (MFT) prediction for the reduced spin susceptibility $\chi^*(t)$ in the paramagnetic state of the system is

$$\chi^*(t) = \frac{\chi_0^*(t)}{1 + \lambda \chi_0^*(t)}, \quad (12a)$$

or equivalently

$$\frac{1}{\chi^*(t)} = \frac{1}{\chi_0^*(t)} + \lambda, \quad (12b)$$

where the MFT coupling constant λ is given by

$$\lambda = \sum_j' \frac{J_{ij}}{J_{\text{max}}}, \quad (12c)$$

the prime on the sum over j signifies that the sum is only taken over exchange bonds J_{ij} from a given spin \mathbf{S}_i to spins \mathbf{S}_j not in the same spin subsystem, and J_{max} is the exchange constant in the system with the largest magnitude. By definition, the expression for $\chi_0^*(t)$ does not contain any of these J_{ij} interactions which are external to a subsystem. Within MFT, Eqs. (12) are correct at each temperature in the paramagnetic state not only for bipartite AF spin systems, but also for any system containing subsystems coupled together by any set of FM and/or AF Heisenberg exchange interactions.

III. MODELING OF EXPERIMENTAL $\chi(T)$ DATA

A. Introduction

We fitted the $\chi(T)$ data per mole of V spins-1/2 in $(\text{VO})_2\text{P}_2\text{O}_7$ by the general expression

$$\chi(T) = \chi_0 + \frac{C_{\text{imp}}}{T - \theta_{\text{imp}}} + \chi^{\text{spin}}(T), \quad (13a)$$

with

$$\chi_0 = \chi^{\text{core}} + \chi^{\text{VV}} \quad (13b)$$

and

$$\begin{aligned} \chi^{\text{spin}}(T) &= \frac{N_A g^2 \mu_B^2}{J_1} \chi^*(t) \\ &= \left(0.3751 \frac{\text{cm}^3 \text{K}}{\text{mol}} \right) \frac{g^2}{J_1/k_B} \chi^* \left(\frac{k_B T}{J_1} \right), \end{aligned} \quad (13c)$$

where N_A is Avogadro's number, μ_B is the Bohr magneton, k_B is Boltzmann's constant and g is the spectroscopic splitting factor (g factor) appropriate to a particular direction of the applied magnetic field with respect to the crystal axes.

The first term χ_0 in Eq. (13a), according to Eq. (13b), is the sum of the nearly isotropic orbital diamagnetic atomic core contribution χ^{core} and the anisotropic orbital paramagnetic Van Vleck contribution χ^{VV} which are normally nearly independent of T . Using the values $\chi^{\text{core}} = -8, -12$ and $-47 \times 10^{-6} \text{ cm}^3/\text{mol}$ for V^{+4} , O^{-2} and $(\text{PO}_4)^{-3}$, respectively,³⁶ we obtain

$$\chi^{\text{core}} = -6.1 \times 10^{-5} \frac{\text{cm}^3}{\text{mol V}} \quad (14)$$

for $(\text{VO})_2\text{P}_2\text{O}_7$. The second term in Eq. (13a) is an extrinsic impurity Curie-Weiss term with impurity Curie constant C_{imp} and Weiss temperature θ_{imp} which gives rise to a low-temperature upturn in $\chi(T)$ which is not predicted by theory for the third term, the intrinsic spin

susceptibility $\chi^{\text{spin}}(T)$, and is assumed to arise from finite chain segments containing an odd number of spins, impurity phase intergrowths in the crystals, paramagnetic impurity phases and/or defects. The C_{imp} and θ_{imp} parameters can be anisotropic if the paramagnetic impurity principal directions are fixed with respect to the crystal axes, as can occur in a single crystal of a material such as studied here in Sec. III D 4, rather than being randomly distributed.

Unless otherwise stated, we assume that the spin susceptibility $\chi^{\text{spin}}(T)$ in Eq. (13a), written in terms of $\chi^*(t, \alpha)$ in Eq. (13c), is the intrinsic spin susceptibility per mole of spins-1/2 in an AF alternating-exchange Heisenberg chain. The explicit expression for $\chi^*(t, \alpha)$ of this chain is given in Ref. 5. In Eq. (13c), J_1 is the larger of the two (J_1 and J_2 with $J_1 > J_2 > 0$) AF alternating exchange constants along the alternating-exchange chain, as denoted in Sec. II above.

One of the parameters entering the calculated spin susceptibility $\chi^{\text{spin}}(T)$ in Eq. (13c) is the g value of the V magnetic moments. Measurements of the anisotropic g values of the spins in both AP-(VO)₂P₂O₇ and HP-(VO)₂P₂O₇ have been carried out using ESR measurements^{17,22} and the results are listed in Table II. The significant differences between the g values of the two phases of (VO)₂P₂O₇ reflect the differences in the local bonding of the V atoms with the coordinating O atoms in the two structures. Comparison of the average g value for HP-(VO)₂P₂O₇ with those for V in the “trellis layer” compounds RV_2O_5 with $R = \text{Ca, Mg and Na}$,^{37–42} also shown in Table II, suggests that the local crystalline electric field (CEF) at the V sites in HP-(VO)₂P₂O₇ is closer to that in these compounds than to the CEF in AP-(VO)₂P₂O₇.

A measure of the goodness of a fit to experimental $\chi(T)$ data is the statistical χ^2 per degree of freedom

TABLE II. g -factors parallel (g_{\parallel}) and perpendicular (g_{\perp}) to the principal local crystalline electric field and/or crystal structure axis and the powder-averaged value $g = \sqrt{(g_{\parallel}^2 + g_{\perp}^2 + g_{\perp}^2)}/3$ for $V^{+4} S = 1/2$ species in several vanadium oxide compounds. Samples are polycrystalline unless otherwise noted. The literature references are given in the last column.

Compound	g_{\parallel}	g_{\perp}	g	Ref.
AP-(VO) ₂ P ₂ O ₇	1.94	1.98	1.97	17
crystal	1.937(a)	1.984(b, c)	1.969	22
HP-(VO) ₂ P ₂ O ₇	1.928(1)(a)	1.974(1)(b),	1.958	32
(crystal)		1.971(1)(c)		
CaV ₂ O ₅			1.957(1)	37
MgV ₂ O ₅			1.96	38
NaV ₂ O ₅ (crystal)	1.938(2)	1.972(2)	1.961(2)	39
crystal	1.936(2)			40
crystal	1.95	1.97	1.96	41
crystal	1.936	1.974, 1.977	1.962	42

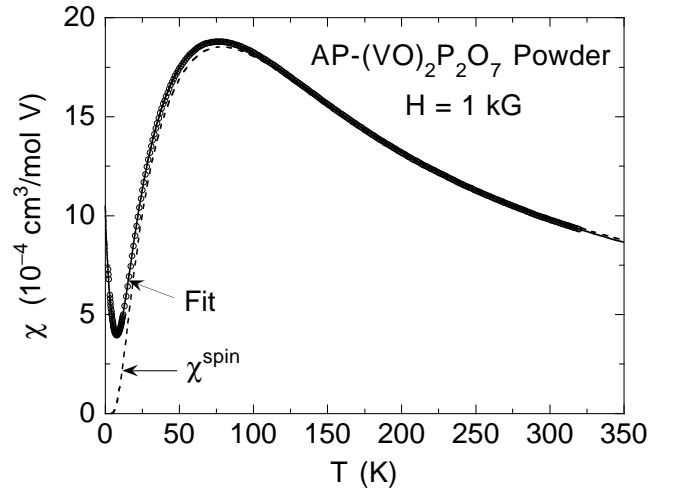


FIG. 4. Magnetic susceptibility χ versus temperature T for a powder sample of AP-(VO)₂P₂O₇ (\circ) from 2 K to 350 K. The solid curve is a two-dimensional fit to the 357 data points using Eq. (13a) assuming a spin susceptibility $\chi^{\text{spin}}(T)$ consisting of those of equal numbers of two independent isolated $S = 1/2$ antiferromagnetic alternating-exchange Heisenberg chains. The dashed curve is the fitted $\chi^{\text{spin}}(T)$. The fitted exchange constants and the derived spin gaps for the two chains are listed in the column labeled “Fit 6” in Table III.

$$\frac{\chi^2}{\text{DOF}} \equiv \frac{1}{N_p - P} \sum_{i=1}^{N_p} [\chi(T_i) - \chi_{\text{fit}}(T_i)]^2, \quad (15)$$

where N_p is the number of data points in the data set and P is the number of independent fitting parameters. This is the quantity that is minimized during our non-linear least-squares fits to experimental $\chi(T)$ data. An additional measure of the quality of a fit is the relative rms deviation σ_{rms} of the fit from the data, given by

$$\sigma_{\text{rms}}^2 \equiv \frac{1}{N_p} \sum_{i=1}^{N_p} \left[\frac{\chi(T_i) - \chi_{\text{fit}}(T_i)}{\chi(T_i)} \right]^2. \quad (16)$$

The fits were all carried out on a 400 MHz Macintosh G3 computer using the software Mathematica 3.0.

B. Magnetic Susceptibility of AP-(VO)₂P₂O₇

1. Powder sample

The purpose of the present section is to test consistency with experimental $\chi(T)$ data of the model of Yamauchi and co-workers for AP-(VO)₂P₂O₇,^{26,27} discussed in the Introduction, in which this compound is proposed to consist magnetically of equal numbers of two independent types of isolated $S = 1/2$ AF alternating-exchange Heisenberg chains with spin gaps of about 35 and 68 K, respectively.

The $\chi(T)$ of a polycrystalline (“powder”) sample of AP-(VO)₂P₂O₇ of mass 172.2 mg and with a moss-green color was measured from 2 to 350 K in a magnetic field of 1 kG and the results are shown as the open circles in Fig. 4. The details of the sample preparation will be presented elsewhere. The color of the sample indicates that it is stoichiometric with a vanadium oxidation state very close to +4.²² The sample was a cylinder of 4 mm diameter and 7 mm length. There was no difference between field-cooled and zero-field-cooled $\chi(T)$ measurements. The quality of the sample, judging from the very small Curie-Weiss upturn at low temperatures due to magnetic impurities and/or defects, is better than previously reported for any powder sample and is about the same as recently reported for a high-quality single crystal²² as shown in Figs. 7 and 8(b) below.

We will describe in detail our modeling results for this sample to indicate how the parameters and the quality of fit change for various types of fits. Similar variations were found from modeling $\chi(T)$ data for two AP-(VO)₂P₂O₇ single crystals below. To make contact with previous modeling of $\chi(T)$ for this material, we first fitted the data by Eqs. (13) assuming that $\chi^{\text{spin}}(T)$ is due to a single type of $S = 1/2$ AF alternating-exchange Heisenberg chain, where the g value is either fixed at the powder-averaged value $g = 1.969$ determined from ESR measurements for AP-(VO)₂P₂O₇ as shown in Table II, yielding “Fit 1”, or allowed to vary during the fit (“Fit 2”). Throughout

the modeling in this section, we use the expression (4) to determine the spin gap from the fitted exchange constants for an alternating-exchange chain. The parameters obtained from each fit are shown in Table III, together with the statistical χ^2/DOF and σ_{rms} for each fit. The defect and/or impurity Curie constant is equivalent to the contribution of about 1.6 mol% with respect to V of spins 1/2 with $g = 2$. The values of the alternating exchange constants J_1 and J_2 and the spin gap Δ are respectively similar in each fit and are about the same as previously estimated from similar fits to $\chi(T)$ data for this compound, respectively (see Table I). Next, we fitted the $\chi(T)$ data using the above model of Yamauchi and co-workers for AP-(VO)₂P₂O₇,^{26,27} but where we constrained the spin gaps to be 36.2 and 66.7 K as found from the inelastic neutron scattering measurements,¹¹ and again either fixed $g = 1.969$ (“Fit 3”) or allowed g to vary during the fit (“Fit 4”). In order to enforce the constraint on the two spin gaps using the expression for $\Delta(\delta)/J$ in Eqs. (4), it was more convenient to use J and δ as the independent parameters in $\chi^{\text{spin}}(T)$ during our least-squares fits instead of J_1 and α . The parameters obtained from the two fits are shown in Table III, together with other parameters derived from the fitted ones. As can be seen from the values of the χ^2/DOF and σ_{rms} , the qualities of the two fits show dramatic improvements over those of Fits 1 and 2 where only a single type of alternating-exchange chain was assumed in the model-

TABLE III. Fitted and derived parameters for $\chi(T)$ of a high-quality powder sample of AP-(VO)₂P₂O₇. A derived quantity is marked by an asterisk (*). A quantity with a “≡” in front of it was constrained to have the value listed and was not fitted. Quantities $A^{(1)}$ and $A^{(2)}$ are quantities associated with two independent isolated chains, respectively. The g value in Fits 1, 3, and 5 were constrained to be the powder-averaged value 1.969 from ESR measurements (see Table II), whereas in Fits 2, 4, and 6 the g value was fitted. Fits 1 and 2 assume a single type of isolated alternating-exchange chain, whereas Fits 3–6 assume the presence of two independent isolated alternating-exchange chains. In Fits 3 and 4 the two respective spin gaps were constrained to have the values found (Ref. 11) from inelastic neutron scattering measurements, whereas in Fits 5 and 6 the two spin gaps were each allowed to vary independently. Our favored fit parameters are those of Fit 6.

Quantity	Fit 1	Fit 2	Fit 3	Fit 4	Fit 5	Fit 6
χ_0 ($10^{-5} \frac{\text{cm}^3}{\text{mol V}}$)	-1.8(1)	-4.5(6)	-1.37(6)	-5.2(1)	-1.99(2)	-2.3(1)
C_{imp} ($10^{-3} \frac{\text{cm}^3 \text{K}}{\text{mol V}}$)	5.8(1)	6.3(2)	3.72(2)	4.52(3)	4.26(2)	4.29(2)
θ_{imp} (K)	-6.4(2)	-6.9(3)	-3.08(4)	-3.95(3)	-3.89(2)	-3.91(2)
g	≡ 1.969	1.993(6)	≡ 1.969	2.006(1)	≡ 1.969	1.972(1)
$J_1^{(1)}/k_B$ (K)	130.9(1)	132.4(4)	137.0(8)*	144.4(4)*	128.7(4)	130.3(7)
$J_1^{(2)}/k_B$ (K)	—	—	122.7(6)*	126.0(4)*	129.9(4)	128.8(5)
$J_2^{(1)}/k_B$ (K)	97.9(2)*	99.8(5)*	118.2(6)*	121.7(3)*	107.6(5)*	109.5(9)*
$J_2^{(2)}/k_B$ (K)	—	—	76.4(5)*	75.2(2)*	83.7(4)*	82.6(6)*
$\alpha^{(1)}$	0.748(1)	0.754(2)	0.863(1)*	0.8728(5)*	0.836(1)	0.840(2)
$\alpha^{(2)}$	—	—	0.622(2)*	0.6178(7)*	0.644(1)	0.641(2)
$J^{(1)}/k_B$ (K)	114.4(2)*	116.1(5)*	127.6(6)*	136.2(4)*	118.1(4)*	119.9(8)*
$J^{(2)}/k_B$ (K)	—	—	99.6(5)*	98.5(2)*	106.8(4)*	105.7(6)*
$\delta^{(1)}$	0.1442(6)*	0.140(1)*	0.0735(5)	0.0679(3)	0.0893(6)*	0.087(1)*
$\delta^{(2)}$	—	—	0.233(1)	0.2363(5)	0.2165(7)*	0.219(2)*
$\Delta^{(1)}/k_B$ (K)	53.6(3)*	53.2(4)*	≡ 36.2	≡ 36.2	38.8(3)*	38.6(5)*
$\Delta^{(2)}/k_B$ (K)	—	—	≡ 66.7	≡ 66.7	67.7(4)*	67.5(5)*
$\frac{\chi^2}{\text{DOF}}$ ($10^{-5} \frac{\text{cm}^3}{\text{mol V}}$) ²	1.31	1.24	0.194	0.0379	0.0130	0.0117
σ_{rms} (%)	1.97	1.94	0.617	0.226	0.138	0.132

ing. However, the g value obtained from Fit 4 is somewhat larger than expected.

Finally, we fitted the same data set in Fig. 4 using the above model of Yamauchi and co-workers for AP-(VO)₂P₂O₇,^{26,27} where we again either fixed $g = 1.969$ (“Fit 5”) or allowed g to vary during the fit (“Fit 6”), but where we did not constrain the fitting parameters J_1 and α of the two independent chains to yield the respective spin gaps found from the inelastic neutron scattering measurements. The fitted parameters are listed for each fit in Table III, together with the statistical χ^2/DOF and σ_{rms} and the derived Δ for each fit. We checked that the identical fitted parameters are obtained for Fit 5 independent of whether the starting parameters are the fitted parameters of Fit 1, for which the exchange constants in the two chains are identical, or of Fit 3 for which they are different. Fit 6 is shown as the solid curve in Fig. 4 and the fitted $\chi^{\text{spin}}(T)$ is shown as the dashed curve.

The fitted and derived parameters for Fits 5 and 6 in Table III exhibit a number of important features. First, the qualities of Fits 5 and 6 to the data are far superior to those of Fits 1 and 2. Second, the values of the alternation parameters and spin gaps for the two independent isolated chains of the model did not converge to the same respective values for the two chains, but rather are clearly differentiated. Third, the fitted g value from Fit 6 is identical within the respective errors with the powder averaged g value in Table II determined from ESR measurements. Fourth, and perhaps most importantly, the two spin gaps derived from the respective exchange constants for the two chains are respectively nearly identical to the two spin gaps found from the single-crystal inelastic neutron scattering measurements by Garrett *et al.*¹¹ and with the values inferred previously by Yamauchi and co-workers from high-field magnetization measurements and a subset of the NMR measurements.^{26,27} It seems very unlikely that the two spin gaps we deduce from this model could be so close to those determined from other independent measurements without the model being essentially correct. The exchange constants and spin gaps we derived from $\chi(T)$ data for the same powder sample in $H = 50$ kG, data which are not otherwise discussed here, are identical within the respective errors to those we obtained above for $H = 1$ kG. Finally, we will see in Sec III D 1 below that when the two-chain model is used to extract the exchange constants within the proposed single-chain high-pressure phase HP-(VO)₂P₂O₇, essentially the same exchange constants and spin gaps are obtained for both chains of the model. This result indicates that our fitting procedure can clearly differentiate between pairs of chains that have the same or different spin gaps, respectively.

We conclude that our analysis of $\chi(T)$ is precisely consistent with the model of Yamauchi and co-workers for the nature of the important spin interactions in AP-(VO)₂P₂O₇. Our values of the spin gaps of the two independent isolated alternating-exchange chains of

the model are in good agreement with those determined from their high-field magnetization and NMR measurements^{26,27} and with the two values determined from the inelastic neutron scattering measurements,¹¹ respectively.

2. MFT analysis of interchain coupling

The neutron scattering measurements on single crystals showed unambiguously that interchain coupling J_a along the a axis of the structure, perpendicular to the alternating-exchange chains and parallel to the legs of the structural two-leg ladders (see Fig. 1), is not negligible.¹¹ However the ratio $|J_a/J_1|$ was estimated from fits to the data to be only 2–3%, where J_1 is the larger of the two exchange couplings along the alternating-exchange chains running along the c axis.¹¹ Another estimate can be obtained as one-half the ratio of the average total dispersion of the two presumed one-magnon bands in the a axis direction [16(4) K] to the one-magnon excitation energy along the direction of the alternating-exchange chains at the zone boundary (180 K), yielding a slightly larger $|J_a/J_1| \approx 4.5(10)\%$. This interchain coupling along the a axis was of course ignored in the fits to the experimental $\chi(T)$ in the previous section. Here we obtain an estimate of the strength of this interchain coupling J_a from analysis of the powder $\chi(T)$ data presented in the previous section. In the absence of accurate calculations of $\chi^*(t)$ for this case, we will utilize the prediction of MFT given in Eqs. (12) for the influence of the interchain coupling on $\chi(T)$.

In order to apply Eqs. (12) to the present modeling framework in which two distinct types of alternating-exchange chains (1) and (2) are assumed to be present, one must appropriately define the “isolated subsystem” discussed in Sec. II. Here, an isolated subsystem consists of one set of the two chains (1) and (2). Thus, the reduced susceptibility of our isolated subsystem is

$$\begin{aligned} \chi_0^* &\equiv \frac{\chi_1^{J_1^{\text{max}}}}{Ng^2\mu_B^2} \\ &= \frac{1}{2} \left[\frac{J_1^{\text{max}}}{J_1^{(1)}} \chi_{\text{chain}}^*(t^{(1)}, \alpha^{(1)}) + \frac{J_1^{\text{max}}}{J_1^{(2)}} \chi_{\text{chain}}^*(t^{(2)}, \alpha^{(2)}) \right] \end{aligned}$$

where

$$t^{(1)} \equiv \frac{k_B T}{J_1^{(1)}}, \quad t^{(2)} \equiv \frac{k_B T}{J_1^{(2)}}, \quad J_1^{\text{max}} \equiv \max [J_1^{(1)}, J_1^{(2)}]. \quad (17)$$

Then the MFT coupling constant λ in Eqs. (12) is, according to Eq. (12c), the average interchain coupling in the a axis direction of a spin in one of the two distinct alternating-exchange chains with all spins in the respective adjacent alternating-exchange chains. Assuming that a spin in each chain is coupled to two nearest

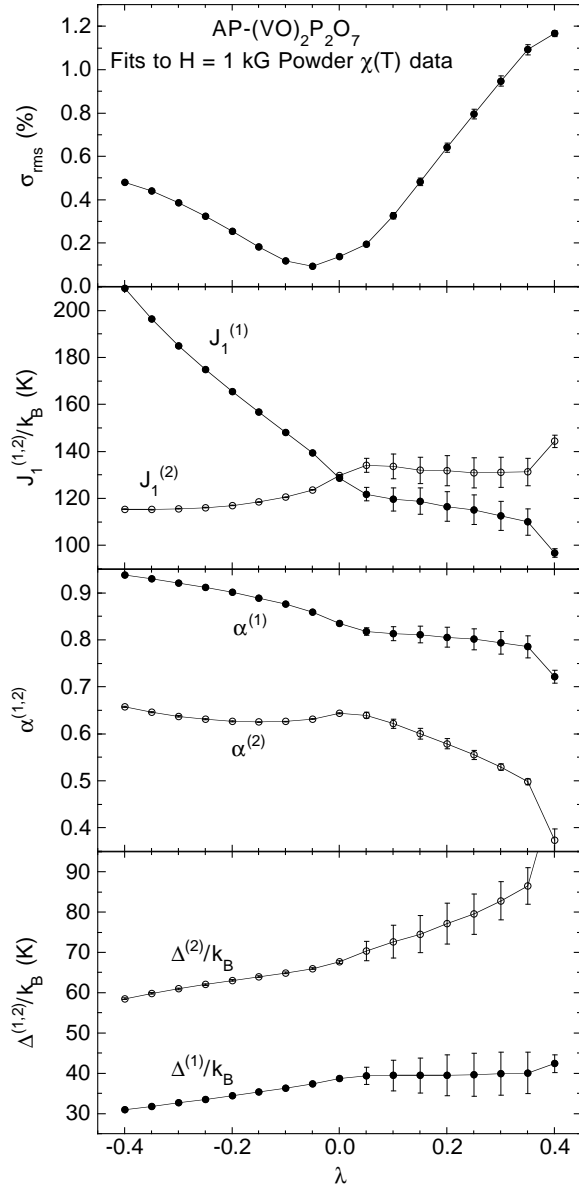


FIG. 5. Parameters $J_1^{(1,2)}$ and $\alpha^{(1,2)}$ and rms deviation σ_{rms} of the fits to the powder $\chi(T)$ data for AP-(VO)₂P₂O₇ in Fig. 4 by MFT for coupled alternating-exchange chains of types (1) and (2) versus the MFT interchain coupling constant λ . A $g = 1.969$ was assumed in all of the fits. The spin gaps $\Delta^{(1,2)}$ for the two distinct chains (1) and (2), derived from the respective $J_1^{(1,2)}$ and $\alpha^{(1,2)}$ values, are also plotted. The lines connecting the data points are guides to the eye.

neighbor spins in the a direction by exchange constant J_a , one obtains

$$\lambda = 2 \frac{J_a}{J_1^{\text{max}}} . \quad (18)$$

We fitted the data in Fig. 4 by Eqs. (13), assuming $g = 1.969$ for all of the fits and using Eqs. (12a), (13c), and (17), where $t \equiv \min(t^{(1)}, t^{(2)})$, to determine the spin susceptibility $\chi^{\text{spin}}(T)$. The resulting fitted pa-

rameters $J_1^{(1,2)}$ and $\alpha^{(1,2)}$ for the chains (1) and (2), the rms deviation σ_{rms} of the fit from the data, and the spin gaps $\Delta^{(1,2)}$ for the chains (1) and (2) derived using Eqs. (4), are plotted versus λ in Fig. 5 for $-0.4 \leq \lambda \leq 0.4$ in λ increments of 0.05, where positive (negative) values of λ correspond to AF (ferromagnetic FM) coupling J_a . Not plotted in Fig. 5 are the fitted values of χ_0 , C_{imp} , and θ_{imp} , which for $\lambda = -0.4, 0$ and 0.4 are $-7.0(1), -1.99(2), 3.8(2) \times 10^{-5} \text{ cm}^3/\text{mol V}$, $4.65(7), 4.26(1), 3.4(1) \times 10^{-3} \text{ cm}^3 \text{ K}/\text{mol V}$, and $-4.0(1), -3.89(2), -3.0(2) \text{ K}$, respectively. From Fig. 5, a pronounced minimum (0.095%) occurs in σ_{rms} at $\lambda \approx -0.05$, which corresponds according to Eq. (18) to a FM J_a with $|J_a/J_1^{(1)}| \approx 0.025$. This is quantitatively consistent with the above-cited estimates¹¹ of this ratio based on a one-chain model with anisotropic (in spin space) spin interactions for the one-magnon dispersion relations observed by inelastic neutron scattering in Ref. 11. The fit to the data for $\lambda = -0.05$ is shown as the solid curve in Fig. 6, where $\chi_0 = -2.50(2) \times 10^{-5} \text{ cm}^3/\text{mol V}$, $C_{\text{imp}} = 0.00428(1) \text{ cm}^3 \text{ K}/\text{mol V}$, $\theta_{\text{imp}} = -3.87(2) \text{ K}$, $J_1^{(1)}/k_B = 139.5(2) \text{ K}$, $\alpha^{(1)} = 0.8597(4)$, $J_1^{(2)}/k_B = 123.7(2) \text{ K}$, $\alpha^{(2)} = 0.6319(6)$, $\Delta^{(1)}/k_B = 37.5(2) \text{ K}$, and $\Delta^{(2)}/k_B = 66.1(2) \text{ K}$. In deriving the spin gap for each chain using Eqs. (4) we have implicitly assumed that the spin gap is unaffected by the interchain couplings.

A somewhat more precise estimate of λ is obtained by allowing this parameter to vary during the fit. The fit parameters and derived spin gaps of the two chains (1) and (2) for the best fit are

$$\chi_0 = -2.37(4) \times 10^{-5} \frac{\text{cm}^3}{\text{mol V}}, \quad C_{\text{imp}} = 0.00427(1) \frac{\text{cm}^3 \text{ K}}{\text{mol V}},$$

$$\theta_{\text{imp}} = -3.87(2) \text{ K}, \quad \lambda = -0.037(4),$$

$$\frac{J_1^{(1)}}{k_B} = 137.1(7) \text{ K}, \quad \alpha^{(1)} = 0.855(2), \quad (19a)$$

$$\frac{J_1^{(2)}}{k_B} = 124.8(4) \text{ K}, \quad \alpha^{(2)} = 0.634(1),$$

$$\frac{\chi^2}{\text{DOF}} = 0.89 \left(10^{-6} \frac{\text{cm}^3}{\text{mol V}} \right)^2, \quad \sigma_{\text{rms}} = 0.099\%,$$

$$\frac{\Delta^{(1)}}{k_B} = 37.8(5) \text{ K}, \quad \frac{\Delta^{(2)}}{k_B} = 66.4(3) \text{ K}.$$

The spin gaps are similar to and may be compared with those for Fit 5 in Table III for the same data, in which $g = 1.969$ was also assumed but where $\lambda = 0$. From Eq. (18) which assumes a nearest neighbor interchain coordination number of 2, we obtain the average interchain coupling strength

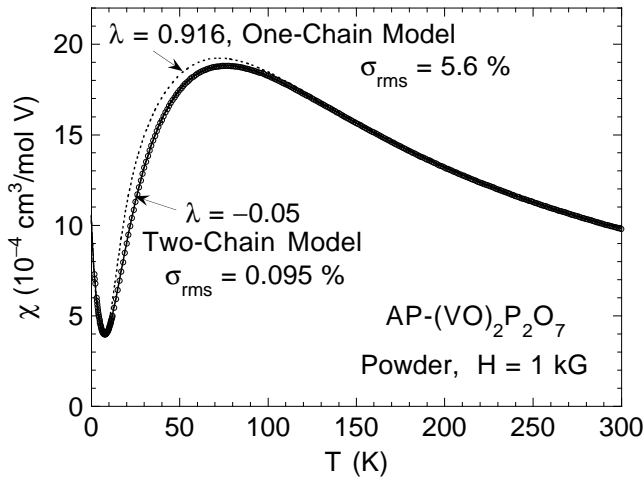


FIG. 6. Magnetic susceptibility χ versus temperature T for a powder sample of $\text{AP}-(\text{VO})_2\text{P}_2\text{O}_7$ (\circ) from Fig. 4. The solid curve is a fit to the data using Eq. (13a) assuming a spin susceptibility $\chi^{\text{spin}}(T)$ consisting of those of equal numbers of two $S = 1/2$ antiferromagnetic alternating-exchange Heisenberg chains which are coupled using MFT with a ferromagnetic coupling constant $\lambda = -0.05$. The dotted curve is the MFT prediction using the exchange constants found for the one-chain model by Uhrig and Normand (Ref. 24), for which the MFT coupling constant is strongly antiferromagnetic with the value $\lambda = 0.916$.

$$\frac{J_a}{k_B} = \frac{\lambda J_1^{(1)}}{2k_B} \approx -2.5 \text{ K} . \quad (19b)$$

As noted in the Introduction, Uhrig and Normand²⁴ proposed a model for $\text{AP}-(\text{VO})_2\text{P}_2\text{O}_7$ in which only one type of alternating-exchange chain occurs and in which the (AF) interchain couplings are given by

$$\frac{J_1}{k_B} = 124 \text{ K}, \quad \alpha = 0.793, \quad \frac{J_a}{J_1} = 0.203, \quad \frac{J_x}{J_1} = 0.255 , \quad (20a)$$

where these parameters were obtained by fitting the one-magnon inelastic neutron scattering dispersion relation data¹¹ for the lower band and using the observed Weiss temperature¹⁰ obtained by fitting experimental $\chi(T)$ data at high temperatures by a Curie-Weiss law (as predicted by MFT). Assuming that the interchain couplings do not affect the spin gap, Eqs. (4) yield

$$\frac{\Delta}{k_B} = 44.0 \text{ K} . \quad (20b)$$

This is about 16% larger than our estimate for $\Delta^{(1)}$ in Eqs. (19a). Of course, since their exchange constants were determined by fitting their theory to the experimental neutron scattering data, their spin gap is the observed value ($\approx 36 \text{ K}$) and not that in Eq. (20b). The discrepancy arises because they find that the spin gap *does* depend on the interchain couplings, as further discussed in Sec. III C below.

Since the interchain spin coordination number for each of the interchain couplings is 2, the value of the MFT interchain coupling constant predicted by Eq. (12c) is

$$\lambda = 2 \left(\frac{J_a}{J_1} + \frac{J_x}{J_1} \right) . \quad (20c)$$

Inserting the parameters of Uhrig and Normand in Eq. (20a) into this equation yields $\lambda = 0.916$. Our fit parameters and their variations with λ in Fig. 5 argue against this very large AF value of λ . To further illustrate the discrepancy within MFT between this one-chain theory and the experimental $\chi(T)$ data, shown as the dotted curve in Fig. 6 is the predicted $\chi(T)$ using $g = 1.969$, the χ_0 , C_{imp} , and θ_{imp} values obtained for $\lambda = -0.05$ in Sec. III B 2, and the MFT prediction for the spin susceptibility in Eqs. (12), where $\chi_0^*(t)$ is that of the isolated alternating-exchange chain for which the exchange constants estimated by Uhrig and Normand in Eq. (20a) were used. The relative deviation of the prediction from the data is $\sigma_{\text{rms}} = 5.6\%$, which is about 60 times larger than the σ_{rms} obtained using the two-chain model for $\lambda = -0.05$. The agreement of both theoretical predictions with the data at high temperatures is expected and in fact is required for either model, since the MFT is most accurate at high temperatures where it yields the Curie-Weiss law. The significant differences between the predictions of the two models only become apparent at the lower temperatures.

In summary, our high-precision fits to the $\chi(T)$ data using the model of two independent chains, in which nearest neighbor chains along the a axis are coupled using MFT, indicate that the average interchain coupling is weakly ferromagnetic, in agreement with the analysis of neutron scattering data by Garrett *et al.*¹¹ using a one-chain model and in disagreement with the one-chain model of Uhrig and Normand²⁴ with strong AF interchain couplings.

3. Single crystals

In this section we analyze the anisotropic $\chi(T)$ data for two single crystals of $\text{AP}-(\text{VO})_2\text{P}_2\text{O}_7$. The data for a small dark green crystal of mass 2.0(1) mg (“crystal 1”), measured in a magnetic field of 5 T using a Quantum Design SQUID magnetometer, have not been reported previously. There was no discernable difference between field-cooled and zero-field-cooled $\chi(T)$ data for this crystal. The data for crystal 2 were reported by Prokofiev *et al.* in Fig. 4(a) of Ref. 22 and were measured in a magnetic field of 2 T. An overview of the anisotropic $\chi(T)$ data for the two crystals is shown in Fig. 7, where the $\chi(T)$ of the powder sample in Fig. 4 is shown for comparison as the dashed curve. The data for the two crystals are in agreement on a coarse scale. The powder averages of the data for both crystals lie above the data for the powder sample for $T \gtrsim 25 \text{ K}$, although in the case

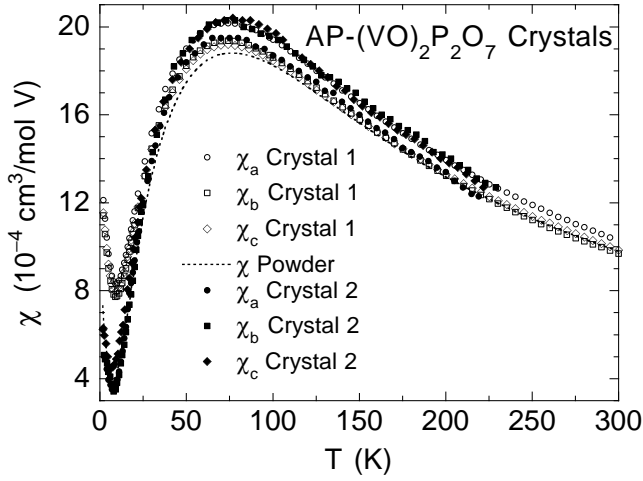


FIG. 7. Overview of the anisotropic magnetic susceptibilities χ versus temperature T for crystals 1 (open symbols) and 2 (filled symbols, from Ref. 22) of $\text{AP}(\text{VO})_2\text{P}_2\text{O}_7$ along the a axis (circles), b axis (squares) and c axis (diamonds). Also shown for comparison is $\chi(T)$ for the powder sample from Fig. 4 (dotted curve).

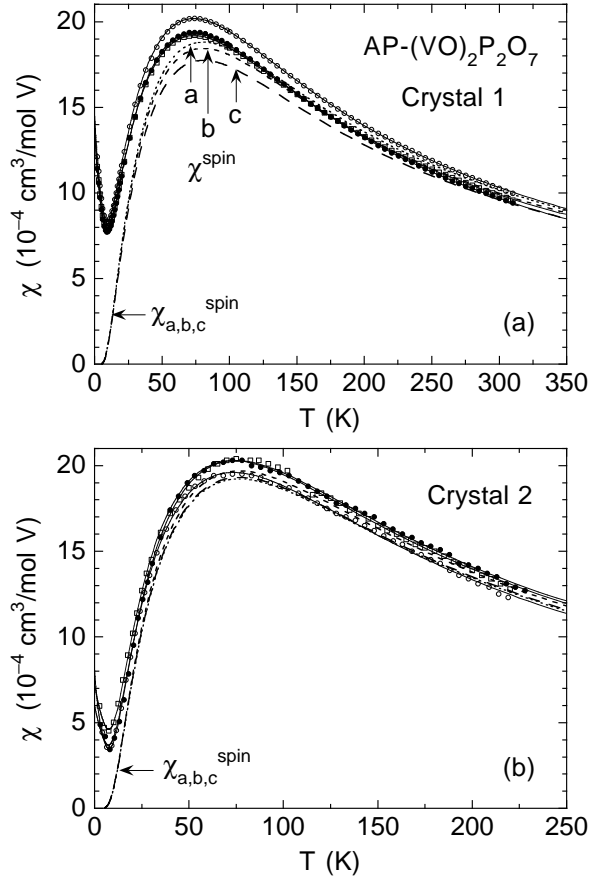


FIG. 8. Fits to the anisotropic magnetic susceptibilities χ versus temperature T for crystals 1 (a) and 2 (Ref. 22) (b) of $\text{AP}(\text{VO})_2\text{P}_2\text{O}_7$. The fits are shown as solid curves and the spin susceptibilities as dashed curves. Note that the temperature scales in (a) and (b) are different.

of crystal 1 this difference is not significant since the uncertainty in the crystal mass is about 5%. Crystal 1 shows a larger Curie-Weiss-type paramagnetic defect and/or impurity contribution at low temperatures than crystal 2. Quantitative differences are seen between the anisotropic $\chi(T)$ for the two crystals. In particular, above about 30 K the $\chi_a(T)$ of crystal 1 agrees with $\chi_{b,c}(T)$ of crystal 2 and $\chi_{b,c}(T)$ of crystal 1 agrees with $\chi_a(T)$ of crystal 2. These qualitative anisotropy differences cannot arise from inaccuracy in, e.g., the crystal masses, which would only affect the respective ordinate scale.

The a -, b - and c -axis $\chi(T)$ data for each crystal in Fig. 7 were fitted simultaneously using Eqs. (13) by writing χ as a diagonal tensor. We assumed the two-chain model for the spin susceptibility of each crystal where the values of J_1 and α for each chain are the same for all three crystal directions, the anisotropic g values are the same for both chains, and allowed χ_0 , C_{imp} and θ_{imp} to be different for each chain and for the three field directions, for a total of 16 fitting parameters. The 4D fits obtained for crystals 1 and 2 are shown as the sets of three solid curves in Figs. 8(a) and 8(b), respectively, and the fitted

TABLE IV. Fitted and derived parameters for the anisotropic $\chi(T)$ of our crystal 1 and for crystal 2 (Ref. 22) of $\text{AP}(\text{VO})_2\text{P}_2\text{O}_7$. A derived quantity is marked by an asterisk (*). Quantities $A^{(1)}$ and $A^{(2)}$ are the quantities associated with two independent isolated chains, respectively.

Quantity	Crystal 1	Crystal 2
χ_{0a} ($10^{-5} \frac{\text{cm}^3}{\text{mol V}}$)	-3.4(3)	-5(3)
χ_{0b} ($10^{-5} \frac{\text{cm}^3}{\text{mol V}}$)	-1.6(2)	0(2)
χ_{0c} ($10^{-5} \frac{\text{cm}^3}{\text{mol V}}$)	-7.7(2)	1(2)
C_{impa} ($10^{-3} \frac{\text{cm}^3 \text{K}}{\text{mol V}}$)	14.9(1)	7.1(5)
C_{impb} ($10^{-3} \frac{\text{cm}^3 \text{K}}{\text{mol V}}$)	14.7(1)	3.7(4)
C_{impc} ($10^{-3} \frac{\text{cm}^3 \text{K}}{\text{mol V}}$)	13.8(1)	7.7(5)
θ_{impa} (K)	-9.85(8)	-10.9(9)
θ_{impb} (K)	-10.06(8)	-4.5(5)
θ_{impc} (K)	-9.73(8)	-10.7(6)
g_a	2.003(2)	1.98(2)
g_b	1.984(2)	2.00(2)
g_c	1.946(2)	1.98(2)
$J_1^{(1)}/k_B$ (K)	122(3)	125(14)
$J_1^{(2)}/k_B$ (K)	143(4)	128(11)
$\alpha^{(1)}$	0.803(9)	0.80(5)
$\alpha^{(2)}$	0.648(6)	0.65(4)
$J_2^{(1)}/k_B$ (K)	98(4)*	101(16)*
$J_2^{(2)}/k_B$ (K)	93(3)*	83(12)*
$J^{(1)}/k_B$ (K)	110(3)*	113(15)*
$J^{(2)}/k_B$ (K)	118(3)*	105(12)*
$\delta^{(1)}$	0.109(5)*	0.11(3)*
$\delta^{(2)}$	0.214(5)*	0.21(2)*
$\Delta^{(1)}/k_B$ (K)	42(3)*	43(11)*
$\Delta^{(2)}/k_B$ (K)	74(3)*	66(10)*
$\frac{\chi^2}{\text{DOF}}$ ($10^{-5} \frac{\text{cm}^3}{\text{mol V}}$) ²	0.0384	2.0
σ_{rms} (%)	0.159	1.61

parameters for both crystals are given in Table IV where the goodnesses of fit for the two crystals are also listed. The anisotropic spin susceptibilities $\chi_\alpha^{\text{spin}}(T)$ were derived using Eq. (13a), i.e., by subtracting the respective χ_0 and defect and/or impurity Curie-Weiss terms from the $\chi(T)$ fit function, and are plotted versus temperature for crystals 1 and 2 as the two sets of three dashed curves in Figs. 8(a) and 8(b), respectively. From Eqs. (13), the only source of anisotropy in $\chi^{\text{spin}}(T)$ is the anisotropy in the g factor. Also listed in Table IV are the spin gaps computed using Eqs. (4) for the two distinct alternating-exchange spin chains in each crystal.

Several features of the data in Table IV are of note. First, as qualitatively expected from Fig. 7, the concentration of paramagnetic defects and/or impurities in crystal 1 is about a factor of two larger than in crystal 2. Second, the spin gaps of the two chains in each of the crystals 1 and 2 are consistent within the error bars with each other and with those found in the above section for the high-quality powder sample of AP-(VO)₂P₂O₇ as listed in Table III. The large error bars on the fitted parameters for crystal 2 arise in large part because the resolution in χ for the data²² above 20 K is only 1×10^{-5} cm³/mol V, which corresponds to a relative resolution of, e.g., 1% at 20 K and 0.5% at 70 K. Third, the fitted g_α values are similar to, but differ in detail from, the corresponding ESR values for AP-(VO)₂P₂O₇ in Table II. These discrepancies between the respective g_α values may originate at least in part from the large Curie-Weiss contribution in crystal 1 and the low resolution of the χ data for crystal 2.

C. Dispersion Relations of AP-(VO)₂P₂O₇

The one-magnon dispersion relation $E(k_c)/J_1$ in the chain direction for the isolated $S = 1/2$ AF alternating-exchange Heisenberg chain, with and without a frustrating second-neighbor coupling, was recently calculated to tenth order in α by Knetter and Uhrig.⁴³ Thus it is possible to make a direct and accurate comparison of the dispersion relations predicted for the two proposed alternating-exchange chains on the basis of our exchange constants in AP-(VO)₂P₂O₇ with those determined by Garrett *et al.*¹¹ using inelastic neutron scattering (INS) measurements. For this comparison, we first use the exchange constants for the two chains from Fit 6 in Table III determined from our fit to the $\chi(T)$ data for the high-purity powder sample using the isolated chain model. The predicted dispersion relations for the two chains are shown as the two solid curves in Fig. 9 where the experimental INS data (●) are also plotted. Also shown as dashed curves are the dispersion relations predicted for the two chains using the intrachain exchange constants in Eq. (19a) found from our fit to the same $\chi(T)$ data by the same two-chain model but where the chains are coupled along the a axis using MFT. The range of our

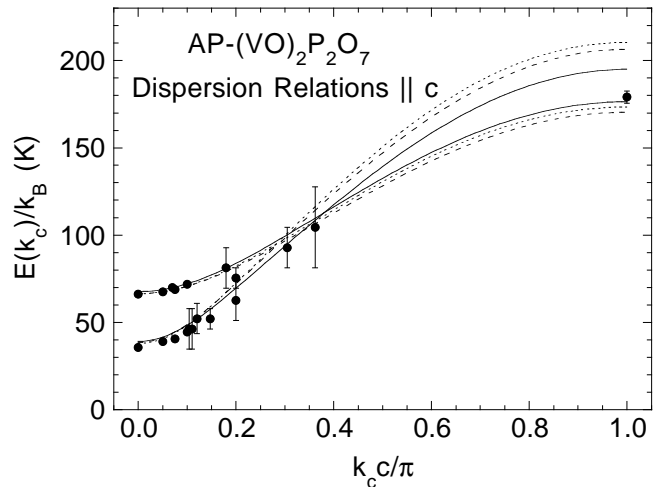


FIG. 9. Comparison of our predicted dispersion relations of the proposed two types of alternating-exchange chains in AP-(VO)₂P₂O₇ with the dispersion relations along the chain direction measured using inelastic neutron scattering at $T = 10$ K by Garrett *et al.* (●, Ref. 11). The two solid curves are the dispersion relations predicted from our exchange constants determined from fits to $\chi(T)$ of a high-purity powder sample by the isolated chain model, and the dashed curves are the corresponding curves for a MFT-coupled chain model. In each case, the dispersion relations were calculated from our intrachain exchange constants using the Fourier series to tenth order in α given by Knetter and Uhrig (Ref. 43). The dotted curve for each chain is the dispersion relation in Eqs. (23) incorporating the interchain coupling according to the model of Uhrig and Normand (Ref. 24).

prediction for the dispersion relation of each chain is thus approximately given by the region between the respective pair of solid and dashed curves.

Our predicted dispersion relations for the two chains agree well with the experimental inelastic neutron scattering data in Fig. 9 except near the zone boundary at $k_c = \pi/c$. Our prediction is that two peaks in the scattered neutron intensity versus energy at this wavevector should be seen with an energy separation of about 20–40 K (≈ 2 –3 meV), contrary to the single data point at this wavevector in Fig. 9. However, the error bar on the data point in Fig. 9 at $k_c = \pi/c$ is only the accuracy of determining the position of the centroid of the neutron scattering peak and is not a direct measure of the width of the peak.²⁸ After most of the fits to the $\chi(T)$ data described in this paper and the determinations of the exchange constants were completed, we learned that recent unpublished INS measurements on a large crystal of AP-(VO)₂P₂O₇ indeed show two peaks at this wavevector with an energy splitting of about 2 meV,²⁸ which partially confirms our prediction. We also predict from Fig. 9 that the dispersion relations of the two chains should cross within the intermediate wavevector regime. We are not aware of experimental INS data that address this aspect of the dispersion relations.

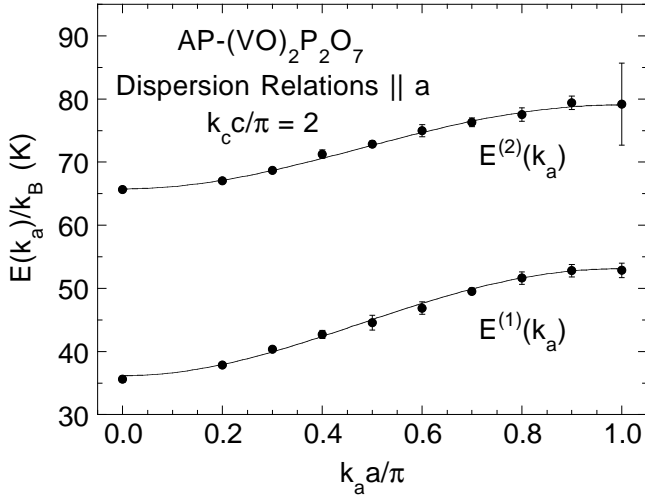


FIG. 10. Fits to the dispersion relations of the proposed two types of alternating-exchange chains in AP-(VO)₂P₂O₇ in the a direction and perpendicular to the chain direction, measured using inelastic neutron scattering at $T = 10$ K by Garrett *et al.* (●, Ref. 11). The two solid curves are fits to the respective data by Eqs. (21), which is the special case for $k_c = 0$ of the general dispersion relation calculated by Uhrig and Normand (Ref. 24).

We note that the two sets of exchange constants in Table IV for the two chains in crystal 1 also predict an energy splitting of the neutron peak at $k_c = \pi/c$, but in this case the predicted dispersion relations of the two chains do not cross. We consider the experimental data and modeling for the high-purity powder sample to be more reliable than for this crystal, for reasons discussed in Sec. III B 3 above, and hence expect that the dispersion relations of the two chains will ultimately be observed to cross.

A quantitative estimate of the interchain couplings J_a and J_x can be obtained by fitting the observed¹¹ dispersion relation for each of the two chains in the a direction, shown in Fig. 10, by the prediction of Uhrig and Normand²⁴

$$E(k_a, k_c = 0) = \Delta(J_1, \alpha, \mu_+, \mu_-) + J_1 \sum_{n=1}^{\infty} a_n(\alpha, \mu_+, \mu_-) [\cos(nk_a a) - 1] \quad (21a)$$

where $\mu_{\pm} \equiv (J_a \pm J_x)/J_1$. To third order in α , μ_- , and/or μ_+ their general dispersion relation yields

$$a_1 = \frac{\mu_-}{4} \left[4 + \alpha(2 + \mu_+) - \alpha^2 - \mu_-^2 \right],$$

$$a_2 = -\frac{\mu_-^2}{8} (2 + 3\alpha + 2\mu_+), \quad a_3 = \frac{\mu_-^3}{8}. \quad (21b)$$

We found that the data in Fig. 10 could not be fitted by Eqs. (21) assuming $J_x = 0$ and $J_a/J_1 \approx -0.019$ as

inferred from $\lambda \approx -0.037$ in Eqs. (19). However, we can still retain this experimentally determined value of λ by allowing J_x to be nonzero. In particular, from Eq. (20c) one obtains $\mu_+ = \lambda/2$. Therefore we set $\mu_+ = -0.019$ and used the experimentally determined values of J_1 and α for each chain in Eq. (19a) in the fit to the respective dispersion relation. This left Δ and μ_- as the only adjustable parameters. We did not use the experimentally determined Δ values in Eqs. (19) because the total width of the experimental dispersion relation for each chain is relatively small and the small difference between the experimental Δ value and the neutron scattering result would give a significant systematic shift to the fit (see also below). The fits are shown as the solid curves in Fig. 10 for chains (1) and (2), respectively, for which the parameters are

$$\frac{J_a^{(1)}}{J_1} = -0.035, \quad \frac{J_x^{(1)}}{J_1} = +0.016, \quad \frac{\Delta^{(1)}}{k_B} = 36.2 \text{ K},$$

$$\frac{J_a^{(2)}}{J_1} = -0.032, \quad \frac{J_x^{(2)}}{J_1} = +0.013, \quad \frac{\Delta^{(2)}}{k_B} = 65.7 \text{ K}. \quad (22)$$

Thus we find that a small but finite AF value of the interchain interaction J_x is necessary to fit the dispersion data perpendicular to the alternating-exchange chains if we retain the fitted λ value in Eqs. (19). Since the nearest-neighbor interchain interaction J_a is ferromagnetic, the next-nearest-neighbor AF interchain interaction J_x is not a geometrically frustrating interaction.

On the other hand, an equally good and nearly identical fit for each chain as shown in Fig. 10 can be obtained assuming that $J_x = 0$ if we relax the above condition on λ . In this case we still use the exchange constants in Eqs. (19) but we set $\mu_- = \mu_+ \equiv \mu$ in the fit to the transverse dispersion data for each chain, yielding the same respective gap values as in Eqs. (22), but where $\mu^{(1)} = -0.050(2)$ and $\mu^{(2)} = -0.044(2)$, so that the $J_a/J_1 = \mu$ and $\lambda = 2\mu \approx -0.10$ values are larger in magnitude than in Eqs. (22).

The dispersion relation parallel to a chain ($\parallel c$) calculated by Uhrig and Normand,²⁴ in which the J_a and J_x interchain couplings are included to third order in α , μ_- , and/or μ_+ , yields

$$E(k_a = 0, k_c) = \Delta + [E_0(k_a = 0, k_c) - E_0(0, 0)] + J_1 \sum_{n=1}^{\infty} b_n(\alpha, \mu_+, \mu_-) [\cos(nk_c c) - 1] \quad (23a)$$

with

$$b_1 = \frac{\mu_- \alpha}{2} \left[1 - \frac{\alpha}{4} + \frac{\mu_+ - \mu_-}{2} \right], \quad b_2 = \frac{3\mu_- \alpha^2}{16}, \quad (23b)$$

where $E_0(0, k_c)$ is the dispersion relation for the isolated alternating-exchange chain to tenth order in α .⁴³ The resulting dispersion relations calculated for the two chains

using Eqs. (23), with the the intrachain exchange constants and spin gaps in Eqs. (19) and the interchain couplings given in Eqs. (22), are shown as the dotted curves in Fig. 9. These are respectively very similar to those for the MFT-coupled chain parameters already plotted as the dashed curves in Fig. 9.

An inconsistency in our fit to the transverse dispersion relation for each chain is that the calculated spin gap is smaller than the observed and fitted one in Fig. 10. The spin gap in Eq. (21a) is given by the third order expansion of Uhrig and Normand²⁴ as

$$\Delta = J_1 \left\{ \frac{\Delta_0(\alpha)}{J_1} + \frac{\mu_-}{4} [4 + \alpha(2 + \mu_+) - \alpha^2] + \frac{\mu_-^2}{8} (4 - 2\alpha + \mu_+) - \frac{\mu_-^3}{8} \right\}, \quad (24)$$

where $\Delta_0(\alpha)/J_1$ is the spin gap in Eqs. (3) or (4) in the absence of interchain coupling. For the exchange constants in Eqs. (19a) and (22) used to fit the transverse dispersion relations in Fig. 10 for chains (1) and (2), from Eq. (24) we obtain $\Delta^{(1)}/k_B = 29.2\text{K}$ and $\Delta^{(2)}/k_B = 59.8\text{K}$, respectively. These spin gaps are each significantly smaller than the fitted ones in Eqs. (22), respectively. These discrepancies arise because the interchain couplings change the spin gap, contrary to our implicit assumption when we fitted the experimental $\chi(T)$ data using the MFT-coupled chain model, so the J_1 and α intrachain exchange parameters for each chain derived from the MFT fit to these data must be considered in the present model to be effective values. The degree to which the effective exchange constants differ from the actual ones is difficult to evaluate. The combined analysis we have done of the susceptibility and dispersion relations is as rigorous as can be done without having in hand an accurate theoretical expression for the spin susceptibility of the system which includes the influence of interchain couplings and concomitant changes in the two spin gaps.

D. Magnetic Susceptibility of HP-(VO)₂P₂O₇

1. Crushed crystals

We begin our modeling of $\chi(T)$ for HP-(VO)₂P₂O₇ using data shown in Fig. 11 which we obtained for a 72.2 mg sample of crushed green transparent single crystals. These data are expected to be more accurate and yield more reliable values of the exchange constants and spin gap than the fits to the data for a powder and for a very small single crystal discussed in the following two sections, respectively. The data were modeled using Eqs. (13) in which $\chi^*(t)$ is the theoretical reduced susceptibility for the $S = 1/2$ AF alternating-exchange Heisenberg chain as proposed by Azuma *et al.*³⁰ The fit

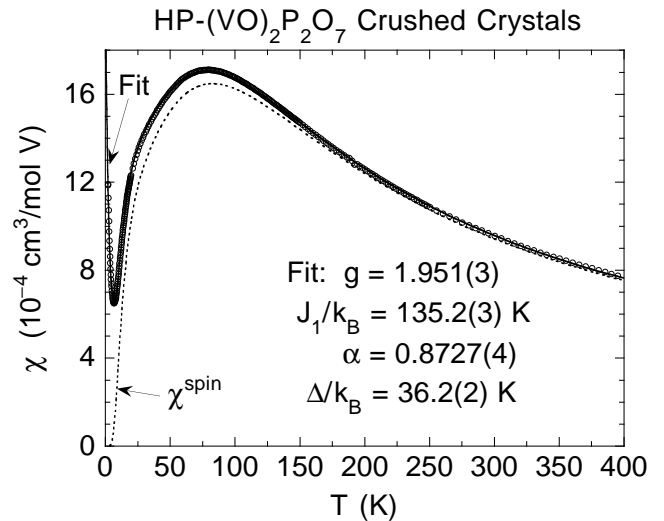


FIG. 11. Magnetic susceptibility χ versus temperature T for a sample of HP-(VO)₂P₂O₇ crushed single crystals (○) from 2 to 400 K. The solid curve is a two-dimensional fit to the 300 data points using Eq. (13a) and the $S = 1/2$ antiferromagnetic alternating-exchange Heisenberg chain model for the intrinsic spin susceptibility $\chi^{\text{spin}}(T)$. The dotted curve is the fitted $\chi^{\text{spin}}(T)$. The fitted values of the g factor, the larger of the two exchange constants in the alternating-exchange chain J_1 , the alternation parameter $\alpha \equiv J_2/J_1$, and the derived spin gap Δ are listed.

TABLE V. Fitted and derived parameters for $\chi(T)$ of crushed single crystals of HP-(VO)₂P₂O₇ obtained using the one-chain and two-chain models. A derived quantity is marked by an asterisk (*). Quantities $A^{(1)}$ and $A^{(2)}$ are the quantities associated with two independent isolated chains, respectively.

Quantity	One-Chain Model	Two-Chain Model
χ_0 ($10^{-5} \frac{\text{cm}^3}{\text{mol V}}$)	-0.1(4)	-1.0(3)
C_{imp} ($10^{-3} \frac{\text{cm}^3 \text{K}}{\text{mol V}}$)	4.88(6)	4.70(4)
θ_{imp} (K)	-1.99(5)	-1.79(3)
g	1.951(3)	1.958(3)
$J_1^{(1)}/k_B$ (K)	135.2(3)	134(14)
$J_1^{(2)}/k_B$ (K)	—	136(14)
$\alpha^{(1)}$	0.8727(4)	0.90(2)
$\alpha^{(2)}$	—	0.85(2)
$J_2^{(1)}/k_B$ (K)	118.0(3)*	120(15)*
$J_2^{(2)}/k_B$ (K)	—	115(15)*
$J^{(1)}/k_B$ (K)	126.6(3)*	127(15)*
$J^{(2)}/k_B$ (K)	—	126(14)*
$\delta^{(1)}$	0.0680(3)*	0.054(10)*
$\delta^{(2)}$	—	0.082(10)*
$\Delta^{(1)}/k_B$ (K)	33.9(2)*	29(7)*
$\Delta^{(2)}/k_B$ (K)	—	39(7)*
$\frac{\chi^2}{\text{DOF}}$ ($10^{-5} \frac{\text{cm}^3}{\text{mol V}}$) ²	0.36	0.16
σ_{rms} (%)	0.58	0.35

is shown as the solid curve in Fig. 11 and the fitted $\chi^{\text{spin}}(T)$ is shown as the dotted curve. The fitted g , J_1 , and α values are listed in the figure, along with the spin gap computed using Eqs. (4). The other parameters of the fit are shown in Table V. The fitted g value is very close to the powder average value 1.958 in Table II obtained from ESR measurements. The impurity Curie constant is equivalent to the contribution of 1.3 mol % with respect to V of spins 1/2 with $g = 2$.

We used the data set in Fig. 11 to estimate typical non-statistical errors that may arise when using the two-chain model to fit the $\chi(T)$ data for AP-(VO)₂P₂O₇ in the above two sections. In addition, if the present one-chain model for HP-(VO)₂P₂O₇ is appropriate, then a fit by the two-chain model should yield very similar exchange constants and spin gaps for the two chains of the model, which ideally would be respectively identical for the two chains. The parameters of the two-chain fit are compared with those of the above single-chain fit in Table V. We see that the fitted parameters of the two chains using the two-chain model are the same within the limits of error with each other and with the parameters of the single-chain model, respectively. This result indirectly confirms that the large differences between the exchange constants and spin gaps found above for the two chains in AP-(VO)₂P₂O₇ are reliable.

2. MFT analysis of interchain coupling

There are no data available for the strength of the interchain coupling in HP-(VO)₂P₂O₇. We estimate this coupling in the same way as in Sec. IIIB2 for AP-(VO)₂P₂O₇. The most precise and accurate $\chi(T)$ data available for HP-(VO)₂P₂O₇ are those for the crushed crystal sample presented and discussed in the previous section. We determined the fitting parameters χ_0 , C_{imp} , θ_{imp} , J_1 , and α as a function of the MFT interchain coupling constant λ over the range $-0.5 \leq \lambda \leq 0.5$, where the fixed $g = 1.958$ was assumed in all these one-chain model fits. The σ_{rms} and the J_1 and α parameters are plotted versus λ in Fig. 12, along with the spin gap Δ determined from J_1 and α using Eqs. (4). At $\lambda = -0.5, 0$, and 0.5 , the fitted parameters χ_0 , C_{imp} , and θ_{imp} were, respectively, $-6.1(2)$, $-0.86(9)$, $3.7(2) \times 10^{-5} \text{ cm}^3/\text{mol V}$, $5.52(9)$, $4.96(4)$, $4.53(8) \times 10^{-3} \text{ cm}^3 \text{ K}/\text{mol V}$, and $-2.33(9)$, $-2.03(4)$, $-1.81(8) \text{ K}$. From the top panel of Fig. 12, the σ_{rms} shows an approximately parabolic variation with λ , with a minimum at $\lambda \approx -0.05$, indicating a weak ferromagnetic interchain coupling as also deduced above for AP-(VO)₂P₂O₇.

We next allowed λ to vary during the fit to determine a more precise value. The fit parameters and derived spin gap of the alternating-exchange chain for the best fit are

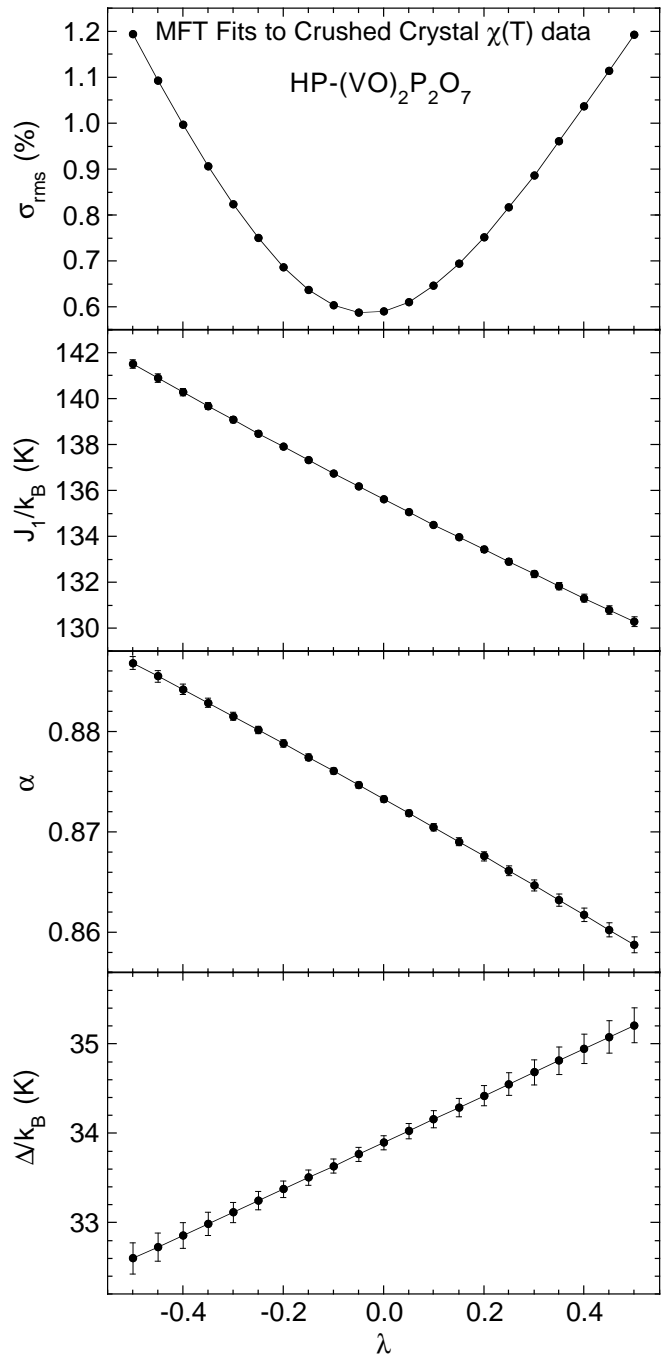


FIG. 12. Parameters J_1 and α and the rms deviation σ_{rms} of the fits to the $\chi(T)$ data for crushed crystals of HP-(VO)₂P₂O₇ in Fig. 11 by MFT for coupled alternating-exchange chains versus the MFT interchain coupling constant λ . A $g = 1.958$ was assumed in all of the fits. The spin gap Δ , derived from the J_1 and α values for each λ , is also plotted versus λ . The error bars are shown for J_1 , α , and Δ . The lines connecting the data points are guides to the eye.

$$\chi_0 = -1.4(2) \times 10^{-5} \frac{\text{cm}^3}{\text{mol V}}, \quad C_{\text{imp}} = 0.00502(4) \frac{\text{cm}^3 \text{K}}{\text{mol V}},$$

$$\theta_{\text{imp}} = -2.06(4) \text{ K}, \quad \lambda = -0.055(14),$$

$$\frac{J_1}{k_B} = 136.2(3) \text{ K}, \quad \alpha = 0.8748(5), \quad (25a)$$

$$\frac{\chi^2}{\text{DOF}} = 0.34 \left(10^{-5} \frac{\text{cm}^3}{\text{mol V}} \right)^2, \quad \sigma_{\text{rms}} = 0.59\%,$$

$$\frac{\Delta}{k_B} = 33.8(2) \text{ K}.$$

The spin gap is identical with that obtained for the one-chain fit in Table V for the same data, in which $g = 1.958$ was also assumed but where $\lambda = 0$, and the other parameters are also very similar, respectively. From Eq. (18), we obtain the average interchain coupling strength

$$J_a = \frac{\lambda J_1}{2k_B} \approx -3.7 \text{ K}. \quad (25b)$$

3. Powder sample: low- T fits

The $\chi(T)$ of a powder sample of $\text{HP}-(\text{VO})_2\text{P}_2\text{O}_7$ was previously reported by Azuma *et al.*,³⁰ shown as the open circles in Fig. 13. A fit of the data up to 30 K by Eqs. (13), where $\chi^*(t)$ is the low- T approximation for the spin susceptibility of a gapped 1D $S = 1/2$ spin system in Eq. (7a), yielded the spin gap $\Delta/k_B = 27 \text{ K}$.³⁰ In this fit, the parameter A in Eq. (7a) was treated as an independently adjustable parameter. In this section we carry out a precise fit of the same data set by Eqs. (13) using the accurately known $\chi^*(t, \alpha)$ spin susceptibility prediction for the $S = 1/2$ AF alternating-exchange Heisenberg chain.⁵ The present fit was carried out in order to compare the fitted parameters respectively obtained from the two types of fits to the same $\chi(T)$ data set for the same sample.

We fitted the $\chi(T)$ data in Fig. 13 using Eqs. (13), where $\chi^*(t, \alpha)$ is that for the $S = 1/2$ AF alternating-exchange Heisenberg chain given in Ref. 5, and with the g value fixed at the spherically-averaged value 1.958 determined from single-crystal anisotropic ESR measurements (see Table II). The resulting fit is shown as the solid curve in Fig. 13, and the fitted spin susceptibility is shown as the dashed curve. The parameters of the fit are

$$\chi_0 = 3.8(3) \times 10^{-5} \frac{\text{cm}^3}{\text{mol V}},$$

$$C_{\text{imp}} = 0.0121(2) \frac{\text{cm}^3 \text{K}}{\text{mol V}}, \quad \theta = -2.6(1) \text{ K},$$

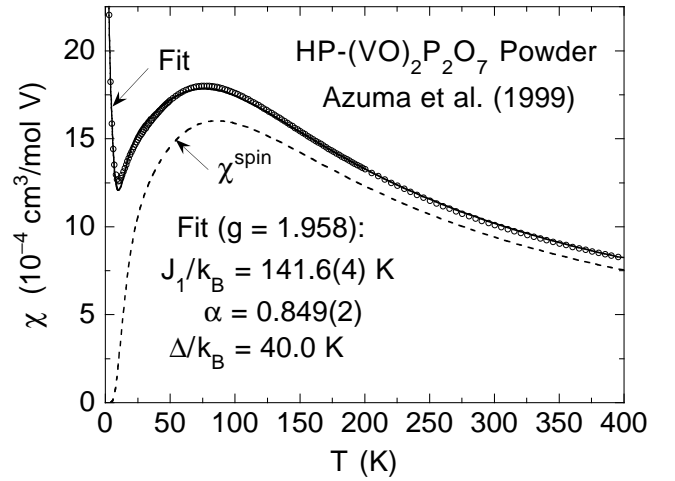


FIG. 13. Magnetic susceptibility χ versus temperature T for a powder sample of $\text{HP}-(\text{VO})_2\text{P}_2\text{O}_7$ (\circ) from 2 K to 400 K (Ref. 30). The solid curve is a two-dimensional fit to the 164 data points using Eq. (13a) and the $S = 1/2$ antiferromagnetic alternating-exchange Heisenberg chain model for the intrinsic spin susceptibility $\chi^{\text{spin}}(T)$, using the powder-averaged g -value of 1.958 determined from ESR measurements. The dashed curve is the fitted $\chi^{\text{spin}}(T)$. The fitted values of the larger of the two exchange constants in the alternating-exchange chain J_1 , the alternation parameter $\alpha \equiv J_2/J_1$ and the derived spin gap Δ are listed.

$$\frac{J_1}{k_B} = 141.6(4) \text{ K}, \quad \alpha = 0.849(2). \quad (26)$$

The C_{imp} value in Eq. (26) is rather large, equivalent to the contribution of 3.2 mol% of spins-1/2 with respect to V and with $g = 2$. Therefore, the fitted prefactor $1/J_1$ to $\chi^*(t)$ in Eq. (13c) could be too small by about 3% if the magnetic species in the impurity phase is $S = 1/2 \text{ V}^{+4}$. On the other hand, if the impurities/defects have a spin larger than 1/2, the influence on the fitted parameters could be much smaller. In order to test this possible influence, we next allowed the g value to be an adjustable parameter in the fit, which has the effect of allowing the amount of V in the $\text{HP}-(\text{VO})_2\text{P}_2\text{O}_7$ phase relative to that in the impurity phase to be variable. The parameters obtained,

$$\chi_0 = 0.0(12) \times 10^{-5} \frac{\text{cm}^3}{\text{mol V}},$$

$$C_{\text{imp}} = 0.0125(3) \frac{\text{cm}^3 \text{K}}{\text{mol V}}, \quad \theta = -2.7(1) \text{ K},$$

$$g = 2.00(1), \quad \frac{J_1}{k_B} = 143.9(8) \text{ K}, \quad \alpha = 0.854(2), \quad (27)$$

are very similar to those obtained in the above fit with fixed g . The fitted value of the prefactor $g^2/(J_1/k_B)$ to $\chi^*(t)$ in Eq. (13c) increased, as anticipated, from 2.71 K^{-1} to 2.77 K^{-1} . Although the fitted g value increased slightly from the value used in the first fit, it is

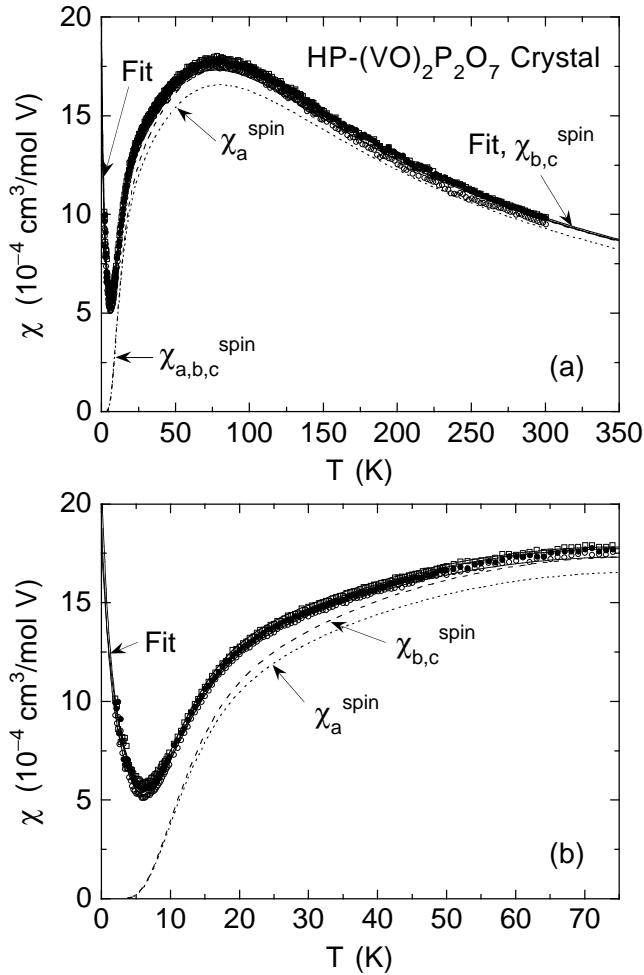


FIG. 14. (a) Magnetic susceptibility χ versus temperature T for single crystal $\text{HP}-(\text{VO})_2\text{P}_2\text{O}_7$ along the a -axis (\circ), b -axis (\bullet) and c -axis (open squares) directions from 2 K to 300 K. (b) Expanded plot of the data in (a) at low temperatures below the broad maximum in $\chi(T)$ at about 75 K. In (a) and (b), the set of three solid curves is a four-dimensional fit to all 885 data points for the a -, b - and c -axis directions using Eq. (13a) and the $S = 1/2$ antiferromagnetic alternating-exchange Heisenberg chain model for the intrinsic spin susceptibility $\chi^{\text{spin}}(T)$. The dashed curves are the fitted $\chi_a^{\text{spin}}(T)$ for the magnetic field along the $\alpha = a$ -axis (short dash) and b - and c -axes (longer dash); the fitted $\chi_b^{\text{spin}}(T)$ and $\chi_c^{\text{spin}}(T)$ are indistinguishable on the scale of the figure.

still close to 2. We conclude that the magnetic impurities and/or defects giving rise to the Curie-Weiss term have little influence on the fitted exchange constants in the $\text{HP}-(\text{VO})_2\text{P}_2\text{O}_7$ phase in the sample.

Taking $J_1/k_B = 142$ K and $\alpha = 0.85$ from Eq. (26), Eq. (3a) yields the spin gap $\Delta/k_B = 40$ K, about 50% larger than the above value of 27 K estimated by Azuma *et al.*³⁰ by fitting the same data up to 30 K (i.e., up to a $T \sim \Delta/k_B$) using the low- T approximation to the spin susceptibility in Eq. (7a). Thus from the respective values of Δ , we find that the error arising from estimat-

ing the gap value by fitting low- T $\chi(T)$ data using the low- T approximation for the spin susceptibility is about 50% in this case. The temperature range over which the low- T approximation is fitted to the experimental data is expected to influence this error (see Sec. III D 5).

4. Single crystal

The $\chi(T)$ data reported by Saito *et al.*³² for a 0.26 mg single crystal of $\text{HP}-(\text{VO})_2\text{P}_2\text{O}_7$ are plotted in Fig. 14. By comparison of these data with those for the powder sample in Fig. 13, the Curie-Weiss impurity and/or defect contribution to $\chi(T)$ for the crystal at low temperatures is seen to be significantly smaller than for the powder sample. From our fit below, we find that it is in fact about a factor of three smaller. This much smaller impurity contribution enhances the reliability of the fitted exchange constants and the derived spin gap obtained from modeling the data for the single crystal. At higher temperatures, the magnitude of the powder-averaged $\chi(T)$ for the single crystal is very similar to the $\chi(T)$ for the powder, as would have been expected.

The modeling of the single-crystal $\chi(T)$ data was carried out in a similar way as for the two crystals of $\text{AP}-(\text{VO})_2\text{P}_2\text{O}_7$ in Sec. III B 3, except that here we use a one-chain model instead of a two-chain model for the spin susceptibility. All 885 data points of the a -, b -, and c -axis $\chi(T)$ data sets in Fig. 14 were fitted simultaneously using Eqs. (13) by writing χ as a diagonal tensor and using the three fixed g values determined for fields along the three principal axis directions from ESR measurements³² as given in Table II above, respectively. With eleven fitting parameters, the data to parameter ratio is 80. The four-dimensional fit obtained is shown as the set of three solid curves in Fig. 14, and the fitted parameters are given in

TABLE VI. Fitted parameters for the anisotropic magnetic susceptibility of single crystal $\text{HP}-(\text{VO})_2\text{P}_2\text{O}_7$ along the a -, b -, and c -axis directions from 2 to 300 K using the one-chain model for the spin susceptibility. Derived quantities are shown with an asterisk (*). The values of J_1 , J_2 , α , J , δ , and Δ are the same for all three crystal axis directions.

Quantity	a -axis	b -axis	c -axis
$\chi_0 (10^{-5} \frac{\text{cm}^3}{\text{mol V}})$	3.4(2)	-0.9(2)	0.0(2)
$C_{\text{imp}} (10^{-3} \frac{\text{cm}^3 \text{K}}{\text{mol V}})$	3.40(6)	3.90(6)	4.39(7)
$\theta_{\text{imp}} (\text{K})$	-2.48(9)	-1.98(8)	-2.75(9)
$J_1/k_B (\text{K})$		131.6(1)	
α		0.8709(5)	
$\chi^{\text{VV}} (10^{-5} \frac{\text{cm}^3}{\text{mol V}})$	9.5*	5.2*	6.1*
$J_2/k_B (\text{K})$		114.6(2)*	
$J/k_B (\text{K})$		123.1(1)*	
δ		0.0690(3)*	
$\Delta/k_B (\text{K})$		33.4(2)*	
$\frac{\chi^2}{\text{DOF}} (10^{-5} \frac{\text{cm}^3}{\text{mol V}})^2$		2.1	
$\sigma_{\text{rms}} (\%)$		1.43	

Table VI along with the goodness of fit. The spin susceptibilities for the three crystal directions are plotted versus temperature in Fig. 14 as dashed curves.

The average of the three fitted C_{imp} values is $3.9 \times 10^{-3} \text{ cm}^3 \text{ K/mol V}$, which is equivalent to the contribution of 1.0 mol% with respect to V of paramagnetic species with $S = 1/2$ and $g = 2$. This contribution is about a factor of three smaller than that found for the powder sample in the previous section. The average of the three θ_{imp} values is -2.0 K , about the same as for the powder sample. The negative sign of θ_{imp} may indicate AF interactions between the defect and/or impurity magnetic moments. The θ_{imp} can also arise from single-impurity-ion CEF effects, and/or as a reflection of partial T -dependent paramagnetic saturation of the paramag-

netic impurities at low temperatures in the fixed field of the measurements. The anisotropic χ^{VV} values are derived from Eqs. (13b) and (14) using the fitted anisotropic χ_0 values in Table VI. The resulting three χ^{VV} values are listed in Table VI.

From the above global fit to the anisotropic $\chi(T)$ data for all three field directions, we find $J_1/k_B = 131.6(1) \text{ K}$ and $\alpha = 0.8709(5)$. The average of the two exchange constants J_1 and J_2 according to Eq. (2d) is $J/k_B = 123.1(1) \text{ K}$, and the alternation parameter expressed in the form of δ is obtained using our J_1 and α values and Eq. (2c) as $\delta = 0.0690(3)$. Using our fitted α and J_1 parameters, Eq. (3a) yields the spin gap $\Delta/k_B = 33.2(2) \text{ K}$. Using the derived J and δ parameters, the more accurate Eqs. (4) predict the spin gap to be $\Delta/k_B = 33.4(2) \text{ K}$,

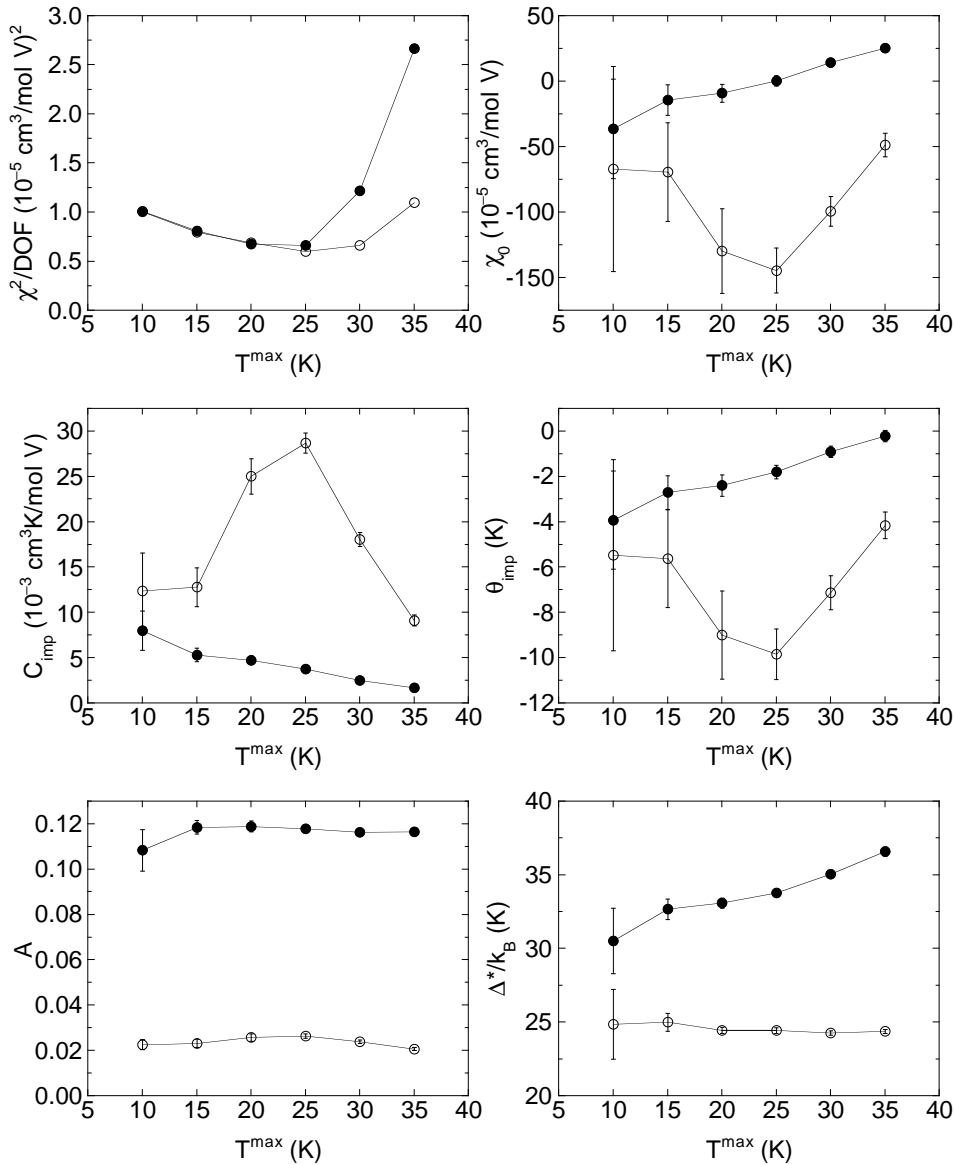


FIG. 15. Parameters obtained from fitting the powder-average $\chi(T)$ data from Fig. 14 for single crystal $\text{HP}-(\text{VO})_2\text{P}_2\text{O}_7$ from 2 K up to a temperature T^{max} by Eqs. (13) using the expressions for the low- T spin susceptibility $\chi^*(t)$ in Eqs. (7a) (\circ , “Fit 1”) and (11) (\bullet , “Fit 2”), respectively.

which is the same to within the error bars as the first estimate.

A summary of all the fitted and derived quantities obtained in this section from our modeling of the $\chi(T)$ measurements for single crystal HP-(VO)₂P₂O₇ is given in Table VI.

5. Powder average of single crystal $\chi(T)$: low- T fits

Additional fits to the powder-averaged single crystal $\chi(T)$ data were carried out at low temperatures to obtain an estimate of the spin gap which is independent of the model for the gapped spin susceptibility. The powder average was used in order to reduce the number of parameters needed to fit the data. We used the general fit expressions (13) in which the spin susceptibility $\chi^*(t)$ is given by the low- T approximations in Eq. (7a) (“Fit 1”) or Eq. (11) (“Fit 2”), and where the prefactor parameter A was fitted independently of the spin gap. The only difference between Fits 1 and 2 is the exponent of $1/t$ in the prefactor to the exponential in the expression for the low- T $\chi^*(t)$, which is $1/2$ for Fit 1 and 1 for Fit 2.

The powder-averaged single-crystal $\chi(T)$ data from Fig. 14 were fitted from 2 K up to a maximum temperature T^{\max} , and the fitted parameters obtained from Fits 1 and 2 are plotted versus T^{\max} in Fig. 15 as open and filled circles, respectively. Also shown in Fig. 15 are the statistical variances (χ^2 per degree of freedom) obtained from both types of fits. The variances for both fits are quite similar and both have a minimum for $T^{\max} \approx 25$ K. However, the impurity Curie constant and Weiss temperature for Fit 1 in Fig. 15 are strongly and nonmonotonically dependent on T^{\max} in contrast to the corresponding dependences for Fit 2. In addition, the values of the fitted χ_0 values for Fit 1 in Fig. 15 are all strongly negative. Since χ_0 cannot be more negative than χ^{core} as estimated above in Eq. (14), because the χ^{VV} in Eq. (13b) is necessarily positive, the Fit 1 fits for all the fitted T^{\max} values are unphysical and hence the other parameters obtained using Fit 1 are most likely also highly inaccurate.

Shown in Fig. 16 are the two optimum fits obtained for $T^{\max} = 25$ K for Fits 1 and 2, respectively, along with the respective fitted spin susceptibilities $\chi^{\text{spin}}(T)$. The $\chi^{\text{spin}}(T)$ for the optimum Fit 1 is highly unlikely, as are the fit parameters as just noted. On the other hand, $\chi^{\text{spin}}(T)$ and the fit parameters for the optimum Fit 2 are reasonable. The values of the fitted parameters for the optimum Fit 2 with $T^{\max} = 25$ K in Fig. 15 are

$$\chi_0 = 0(4) \times 10^{-5} \frac{\text{cm}^3}{\text{mol V}},$$

$$C_{\text{imp}} = 0.0038(4) \frac{\text{cm}^3 \text{K}}{\text{mol V}}, \quad \theta = -1.8(3) \text{ K},$$

$$A = 0.118(2) \frac{\text{cm}^3 \text{K}}{\text{mol V}}, \quad \frac{\Delta}{k_B} = 33.8(2) \text{ K}. \quad (28)$$

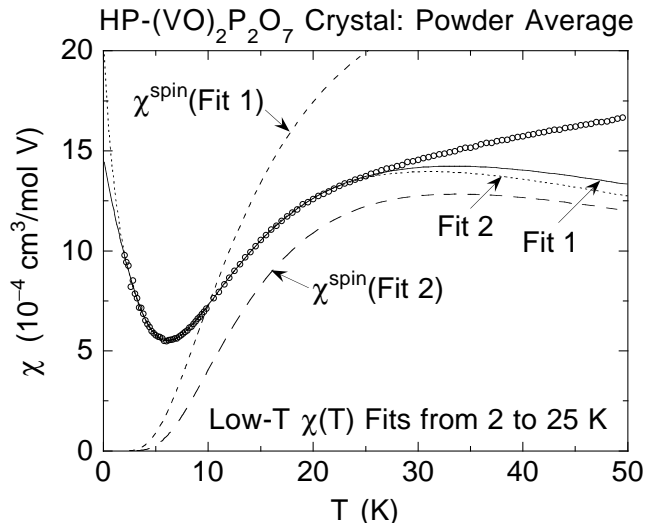


FIG. 16. Powder-averaged magnetic susceptibility χ versus temperature T below 50 K from Fig. 14 for single crystal HP-(VO)₂P₂O₇ (○). The solid and dotted curves are Fits 1 and 2 to the data from 2 to 25 K using the low- T approximations for the spin susceptibility in Eqs. (7a) and (11), respectively. The corresponding fitted spin susceptibilities $\chi^{\text{spin}}(T)$ are shown as short- and long-dashed curves, respectively. Extrapolations of the curves to lower and higher temperatures are also shown.

The first three parameters are very close to the corresponding powder-averaged anisotropic single crystal values in Table VI which were obtained in the above section assuming the $S = 1/2$ AF alternating-chain Heisenberg model for the spin susceptibility, and the two spin gaps are nearly identical. The agreement between the spin gaps found from the two independent fits supports the applicability of this spin Hamiltonian to the spin system in HP-(VO)₂P₂O₇.

IV. SUMMARY AND CONCLUSIONS

We have carried out detailed modeling studies of the magnetic susceptibilities $\chi(T)$ of powder and single crystal samples of the ambient- and high-pressure phases of (VO)₂P₂O₇. The major goal of the modeling was to determine whether the recent proposals of a two-chain model for AP-(VO)₂P₂O₇ (Refs. 26 and 27) and a single-chain model for HP-(VO)₂P₂O₇ (Ref. 30) are consistent with the respective experimental $\chi(T)$ data. Using the high-accuracy theoretical $\chi^*(t, \alpha)$ function for isolated $S = 1/2$ AF alternating-exchange Heisenberg chains in Ref. 5, high precision tests of these models were possible.

The $\chi(T)$ data for each phase were first analyzed using the AF alternating-exchange chain model for *isolated* chains. We found that the proposed models are strongly supported by our high-precision fits to the $\chi(T)$ data for each phase, from which the exchange constants and spin gap of each type of chain in each phase were de-

terminated. We then considered the case of *coupled* chains. The influences of interchain couplings on the values of the intrachain exchange constants and the spin gap of each type of chain in the two phases were evaluated from additional fits to the $\chi(T)$ data where the interchain coupling was treated in the molecular field approximation. For both phases, we find that the interchain molecular field coupling constant is weakly ferromagnetic with a value $\lambda \approx -0.05$, in agreement with Ref. 11 and in disagreement with Ref. 24. Assuming that the interchain coordination number is two and using the values of λ and the intrachain exchange constants, the interchain exchange coupling constant along the a axis direction is computed to be $J_a/k_B \approx -3.0(5)$ K in both phases of $(\text{VO})_2\text{P}_2\text{O}_7$. Thus although our modeling of $\chi(T)$, from which the intrachain exchange constants and spin gaps were derived, did not explicitly incorporate the influence of the magnon dispersion perpendicular to the chain direction, we believe that our mean-field treatment effectively captures most of these effects on $\chi(T)$ since the interchain coupling is found to be very weak compared to the intrachain couplings. This supposition is confirmed by our fit to the low- T powder-averaged data for a single crystal of $\text{HP}-(\text{VO})_2\text{P}_2\text{O}_7$ by a model-independent low- T approximation for the spin susceptibility of a 1D spin system, which yielded a spin gap of 33.8(2) K that is identical within the error bars to the spin gap of 33.4(2) K obtained from a fit to the three complete anisotropic $\chi(T)$ data sets for the crystal using the $\chi^*(t)$ spin susceptibility function for the alternating-exchange chain. The good agreement of the respective spin gaps with those in Table I obtained from inelastic neutron scattering and NMR measurements also supports the magnetic models that we have used for the two phases.

According to the usual simple model for d orbitals of transition metal atoms in a distorted octahedral crystalline electric field, the value of the Van Vleck susceptibility χ^{VV} increases as the deviation of the g value from the free-electron value of 2 increases. Thus from the g values determined by ESR for $\text{HP}-(\text{VO})_2\text{P}_2\text{O}_7$ in Table II, one would predict that $\chi_a^{\text{VV}} > \chi_c^{\text{VV}} \gtrsim \chi_b^{\text{VV}}$ for this phase. This expectation is borne out by the values of χ^{VV} in Table VI for a high-quality single crystal of this phase. This agreement further supports our conclusion that the $\chi(T)$ data are consistent with the presence of a single type of $S = 1/2$ AF alternating-exchange Heisenberg chain in this phase. The powder average of our χ^{VV} values in Table II is close to the value $6 \times 10^{-5} \text{cm}^3/\text{mol V}$ estimated from $\chi(T)$ and $^{31}\text{K}(T)$ NMR measurements by Kikuchi *et al.*¹⁶ for $\text{AP}-(\text{VO})_2\text{P}_2\text{O}_7$.

Additional confirmation of the two-chain model for $\text{AP}-(\text{VO})_2\text{P}_2\text{O}_7$ is the agreement we find between our predicted one-magnon dispersion relations in the chain direction for the two chains with the results of inelastic neutron scattering measurements at small and large wavevectors. In the intermediate wavevector regime, our calculated dispersion relations of the respective chains predict that they should cross. To our knowledge, there

are no relevant inelastic neutron scattering data yet with which to test this prediction. With the caveat given in the next paragraph, our final estimates of the intrachain exchange constants and of the spin gaps of the respective alternating-exchange chains in the two phases are given in Table I, where the error bars on each quantity take our mean-field modeling of interchain interactions into account.

By fitting the experimental dispersion relations *perpendicular* to the two chains in $\text{AP}-(\text{VO})_2\text{P}_2\text{O}_7$ of Garrett *et al.*¹¹ by the theoretical predictions of Uhrig and Normand²⁴ which incorporate the influence of interchain couplings, both of the couplings J_a and J_\times were found to be small but nonnegligible. In addition, the theoretical dispersion relations²⁴ show that these couplings change the spin gap from that of an isolated chain with the same intrachain exchange constants, whereas our modeling of the experimental $\chi(T)$ data including the influence of the interchain coupling in a mean-field approximation implicitly assumed that the interchain couplings do not change the spin gap. Using our interchain exchange constants obtained from fitting the experimental dispersion relations perpendicular to the chains¹¹ using their theory and using our intrachain exchange constants obtained from modeling the experimental $\chi(T)$ data, the spin gap of each chain was calculated using their theory to be significantly smaller than the actual spin gap for each chain. Thus the intrachain exchange constants we obtain from the mean-field treatment of the interchain coupling should be considered to be effective values within this model. An improved evaluation of the exchange constants from $\chi(T)$ data will only be possible using a theoretical expression for $\chi(T)$ which incorporates the effects of the interchain couplings on the two spin gaps.

The spin gap of $\text{HP}-(\text{VO})_2\text{P}_2\text{O}_7$ obtained from analyzing $\chi(T)$ data using the low- T approximation³⁴ $\chi^*(t) = (A/\sqrt{t}) \exp(-\Delta^*/t)$ [Eq. (7a)] is found to be different than obtained using the above high-accuracy theoretical $\chi^*(t, \alpha)$ function for alternating-exchange chains to analyze the same data. For example, from a comparison of the spin gap obtained previously for a powder sample of $\text{HP}-(\text{VO})_2\text{P}_2\text{O}_7$ using this approximation³⁰ with the spin gap we obtained from a fit to the same data set using the accurate $\chi^*(t, \alpha)$ function, we infer that the error involved in determining the spin gap using this low- T approximation is about 50% in this case. Similar discrepancies have been found previously when analyzing $\chi(T)$ data for 1D spin systems in a similar way. In the compound SrCu_2O_3 , for example, the spin gap of the $S = 1/2$ Cu^{+2} two-leg ladders within the Cu_2O_3 trellis layers obtained by fitting $\chi(T)$ data up to temperatures $T \sim \Delta/k_B$ using Eq. (7a) (assuming that A is an independently adjustable parameter) yielded $\Delta/k_B = 420$ K,⁴⁴ whereas inelastic neutron scattering measurements on this compound yielded $\Delta/k_B \approx 380$ K.^{45,46} On the other hand, we found that the low- T approximation $\chi^*(t) = (A/t) \exp(-\Delta^*/t)$, in which the power of t in the

prefactor to the exponential is modified, can yield much more accurate values of the spin gap.

Our AF exchange constants in Table I along the alternating-exchange V chains in the two phases of $(\text{VO})_2\text{P}_2\text{O}_7$ are of the same order as the nearest-neighbor exchange interactions estimated experimentally³ and theoretically⁴⁷ between the V ions in the two-leg ladder compound MgV_2O_5 , but are much smaller than the value of 660–670 K found^{3,37,47,48} for the V-V coupling across the ladder rungs in isostructural CaV_2O_5 . Korotin *et al.* have inferred theoretically that the large differences between the exchange constants in the latter two compounds arise from the stronger tilting of the VO_5 square pyramids in MgV_2O_5 as compared to CaV_2O_5 .⁴⁹ The conventional empirical rules for estimating the strengths of nearest-neighbor superexchange interactions in oxides are strongly violated in CaV_2O_5 and also in cuprate spin ladder compounds, as extensively discussed in Ref. 3. A similar analysis of the exchange coupling strengths in the two phases of $(\text{VO})_2\text{P}_2\text{O}_7$ would be informative and perhaps quite relevant to a more general evaluation of this issue.

ACKNOWLEDGMENTS

We thank S. E. Nagler and G. S. Uhrig for helpful discussions and correspondence, and our recent collaborators in Ref. 5 on work which made the present study possible. We are grateful to H. Schwenk for the anisotropic $\chi(T)$ data for a single crystal of AP- $(\text{VO})_2\text{P}_2\text{O}_7$ in Fig. 4(a) of Ref. 22, designated as “crystal 2” in the present paper, to S. E. Nagler for sending the dispersion relation data for AP- $(\text{VO})_2\text{P}_2\text{O}_7$ in Fig. 3 of Ref. 11, and to C. Knetter for sending the expansion coefficients for the dispersion relation of the frustrated alternating-exchange chain in Ref. 43 prior to publication. Ames Laboratory is operated for the U.S. Department of Energy by Iowa State University under Contract No. W-7405-Eng-82. The work at Ames Laboratory was supported by the Director for Energy Research, Office of Basic Energy Sciences. This work was partly supported by CREST (Core Research for Evolutional Science and Technology) of Japan Science and Technology Corporation (JST) and Grant-in-Aid for Scientific Research of the Ministry of Education, Science, Sports and Culture, Japan.

- ¹ For reviews, see: M. A. Kastner, R. J. Birgeneau, G. Shirane, and Y. Endoh, *Rev. Mod. Phys.* **70**, 897 (1998); D. C. Johnston, in *Handbook of Magnetic Materials*, edited by K. H. J. Buschow (Elsevier, Amsterdam, 1997), Vol. 10, Chap. 1, pp. 1–237; D. C. Johnston, *J. Magn. Magn. Mater.* **100**, 218 (1991).
- ² For reviews, see: D. C. Johnston, in Ref. 1; E. Dagotto, cond-mat/9908250; *Repts. Prog. Phys.* **62**, 1525 (1999); T. M. Rice, *Z. Phys. B* **103**, 165 (1997); H. Tsunetsugu, *Physica B* **237–238**, 108 (1997); E. Dagotto and T. M. Rice, *Science* **271**, 618 (1996); M. Takano, *Physica C* **263**, 468 (1996); S. Maekawa, *Science* **273**, 1515 (1996); G. Chaboussant, M.-H. Julien, Y. Fagot-Revurat, M. Hanson, L. P. Lévy, C. Berthier, M. Horvatić, and O. Piovesana, *Eur. Phys. J. B* **6**, 167 (1998).
- ³ D. C. Johnston, M. Troyer, S. Miyahara, D. Lidsky, K. Ueda, M. Azuma, Z. Hiroi, M. Takano, M. Isobe, Y. Ueda, M. A. Korotin, V. I. Anisimov, A. V. Mahajan, and L. L. Miller, cond-mat/0001147 (unpublished).
- ⁴ For a review and extensive bibliography of the experimental and theoretical work on NaV_2O_5 , see Ref. 5.
- ⁵ D. C. Johnston, R. K. Kremer, M. Troyer, X. Wang, A. Klümper, S. L. Bud’ko, A. F. Panchula, and P. C. Canfield, *Phys. Rev. B* (in press).
- ⁶ J. W. Johnson, D. C. Johnston, and A. J. Jacobson, in *Preparation of Catalysts IV*, edited by B. Delmon, P. Grange, P. A. Jacobs, and G. Poncelet (Elsevier, Amsterdam, 1987), pp. 181–190, and cited references.
- ⁷ P. L. Gai and K. Kourtakis, *Science* **267**, 661 (1995), and cited references.
- ⁸ Yu. E. Gorbunova and S. A. Linde, *Dokl. Akad. Nauk SSSR* **245**, 584 (1979).
- ⁹ J. W. Johnson, D. C. Johnston, A. J. Jacobson, and J. F. Brody, *J. Am. Chem. Soc.* **106**, 8123 (1984).
- ¹⁰ D. C. Johnston, J. W. Johnson, D. P. Goshorn, and A. J. Jacobson, *Phys. Rev. B* **35**, 219 (1987). See also: D. C. Johnston and J. W. Johnson, *J. Am. Chem. Soc.*, *Chem. Commun.*, 1720 (1985).
- ¹¹ A. W. Garrett, S. E. Nagler, D. A. Tennant, B. C. Sales, and T. Barnes, *Phys. Rev. Lett.* **79**, 745 (1997).
- ¹² P. T. Nguyen, R. D. Hoffman, and A. W. Sleight, *Mater. Res. Bull.* **30**, 1055 (1995).
- ¹³ Z. Hiroi, M. Azuma, Y. Fujishiro, T. Saito, M. Takano, F. Izumi, T. Kamiyama, and T. Ikeda, *J. Solid State Chem.* **146**, 369 (1999).
- ¹⁴ T. Barnes and J. Riera, *Phys. Rev. B* **50**, 6817 (1994).
- ¹⁵ Y. Furukawa, A. Iwai, K. Kumagai, and A. Yakubovskiy, *J. Phys. Soc. Jpn.* **65**, 2393 (1996).
- ¹⁶ J. Kikuchi, T. Yamauchi, and Y. Ueda, *J. Phys. Soc. Jpn.* **66**, 1622 (1997).
- ¹⁷ H. Schwenk, M. Sieling, D. König, W. Palme, S. A. Zvyagin, B. Lüthi, and R. S. Eccleston, *Solid State Commun.* **100**, 381 (1996).
- ¹⁸ R. S. Eccleston, T. Barnes, J. Brody, and J. W. Johnson, *Phys. Rev. Lett.* **73**, 2626 (1994).
- ¹⁹ B. Wolf, S. Schmidt, H. Schwenk, S. Zherlitsyn, and B. Lüthi (unpublished).
- ²⁰ M. Grove, P. Lemmens, G. Güntherodt, B. C. Sales, F. Büllsfeld, and W. Assmus, cond-mat/9912050 (unpublished); *Phys. Rev. B* **61**, 6126 (2000).

- ²¹ A. W. Garrett, S. E. Nagler, T. Barnes, and B. C. Sales, *Phys. Rev. B* **55**, 3631 (1997).
- ²² A. V. Prokofiev, F. Büllersfeld, W. Assmus, H. Schwenk, D. Wichert, U. Löw, and B. Lüthi, *Eur. Phys. J. B* **5**, 313 (1998).
- ²³ D. A. Tennant, S. E. Nagler, A. W. Garrett, T. Barnes, and C. C. Torardi, *Phys. Rev. Lett.* **78**, 4998 (1997).
- ²⁴ G. S. Uhrig and B. Normand, cond-mat/9807186 (unpublished); *Phys. Rev. B* **58**, R14705 (1998). The expressions for the hopping coefficients t_{11} and t_{20} in Eq. (1) of this paper are incorrect (G. S. Uhrig, private communication). In the notation of the present paper, where our α is the same as their λ , the correct expressions are $t_{11} = (\alpha\mu_-/8)[1 - (\alpha/4) + \mu_+/2]$ and $t_{20} = -(\alpha^2/32)(1 + \alpha/2)$. We have used the correct expressions in the present paper.
- ²⁵ A. Weiße, G. Bauzera, and H. Fehski, cond-mat/9805374 (unpublished); *Eur. Phys. J. B* **7**, 5 (1999).
- ²⁶ T. Yamauchi, Y. Narumi, J. Kikuchi, Y. Ueda, K. Tatani, T. C. Kobayashi, K. Kindo, and K. Motoya, *Phys. Rev. Lett.* **83**, 3729 (1999).
- ²⁷ J. Kikuchi, K. Motoya, T. Yamauchi, and Y. Ueda, cond-mat/9902205 (unpublished); *Phys. Rev. B* **60**, 6731 (1999).
- ²⁸ M. Enderle, S. E. Nagler, H. Schwenk, B. Lüthi, and W. Assmus, Centennial Meeting of the Am. Phys. Soc., Atlanta, GA, 20–26 March 1999, Abstract YC36.03; S. E. Nagler (private communication).
- ²⁹ K. Damle and S. E. Nagler, cond-mat/9904438 (unpublished); Centennial Meeting of the Am. Phys. Soc., Atlanta, GA, 20–26 March 1999, Abstract YC36.04.
- ³⁰ M. Azuma, T. Saito, Y. Fujishiro, Z. Hiroi, M. Takano, F. Izumi, T. Kamiyama, T. Ikeda, Y. Narumi, and K. Kindo, *Phys. Rev. B* **60**, 10 145 (1999).
- ³¹ D. C. Johnston, *Phys. Rev. B* **54**, 13 009 (1996).
- ³² T. Saito, T. Terashima, M. Azuma, M. Takano, T. Goto, H. Ohta, W. Utsumi, P. Bordet, and D. C. Johnston (unpublished).
- ³³ T. Barnes, J. Riera, and D. A. Tennant, cond-mat/9801224 (unpublished); *Phys. Rev. B* **59**, 11 384 (1999).
- ³⁴ M. Troyer, H. Tsunetsugu, and D. Würtz, *Phys. Rev. B* **50**, 13 515 (1994).
- ³⁵ L. N. Bulaevskii, *Sov. Phys. Solid State* **11**, 921 (1969) [*Fiz. Tverd. Tela* **11**, 1132 (1969)].
- ³⁶ E. König and G. König, in *Landolt-Börnstein*, Vol. 10-2, edited by K.-H. Hellwege and A. M. Hellwege (Springer-Verlag, Berlin, 1979), pp. 12–13.
- ³⁷ M. Onoda and N. Nishiguchi, *J. Solid State Chem.* **127**, 359 (1996).
- ³⁸ M. Onoda and A. Ohyama, *J. Phys.: Condens. Matter* **10**, 1229 (1998).
- ³⁹ A. N. Vasil'ev, A. I. Smirnov, M. Isobe, and Y. Ueda, *Phys. Rev. B* **56**, 5065 (1997).
- ⁴⁰ S. Schmidt, W. Palme, B. Lüthi, M. Weiden, R. Hauptmann, and C. Geibel, *Phys. Rev. B* **57**, 2687 (1998).
- ⁴¹ M. Lohmann, A. Loidl, M. Klemm, G. Obermeier, and S. Horn, *Solid State Commun.* **104**, 649 (1997).
- ⁴² M. Onoda and T. Kagami, *J. Phys.: Condens. Matter* **11**, 3475 (1999).
- ⁴³ C. Knetter and G. S. Uhrig, cond-mat/9906243 (unpublished); *Eur. Phys. J. B* **13**, 209 (2000).
- ⁴⁴ M. Azuma, Z. Hiroi, M. Takano, K. Ishida, and Y. Kitaoka, *Phys. Rev. Lett.* **73**, 3463 (1994).
- ⁴⁵ M. Azuma, M. Takano, and R. S. Eccleston, *J. Phys. Soc. Jpn.* **67**, 740 (1998).
- ⁴⁶ R. S. Eccleston, M. Uehara, J. Akimitsu, H. Eisaki, N. Motoyama, and S. Uchida, *Phys. Rev. Lett.* **81**, 1702 (1998).
- ⁴⁷ M. A. Korotin, I. S. Elfimov, V. I. Anisimov, M. Troyer, and D. I. Khomskii, cond-mat/9901214 (unpublished); *Phys. Rev. Lett.* **83**, 1387 (1999).
- ⁴⁸ S. Miyahara, M. Troyer, D. C. Johnston, and K. Ueda, *J. Phys. Soc. Jpn.* **67**, 3918 (1998).
- ⁴⁹ M. A. Korotin, V. I. Anisimov, T. Saha-Dasgupta, and I. Dasgupta, *J. Phys.: Condens. Matter* **12**, 113 (2000).